NASA Contractor Report
159385

Laser Angle Sensor Development

C.R. Pond, P.D. Texeira
Boeing Aerospace Company
Seattle, Washington 98124

Contract NAS1-15987
October 1980

National Aeronautics and
Space Administration

Langley Research Center
Hampton, Virginia 23665

NASA Contractor Report
159385

Laser Angle Sensor Development

C.R. Pond, P.D. Texeira
Boeing Aerospace Company
Seattle, Washington 98124

Contract NAS1-15987
October 1980

NASA

TABLE OF CONTENTS

LIST OF ILLUSTRATIONS

LIST OF ILLUSTRATIONS (Continued)

LIST OF TABLES

LASER ANGLE SENSOR DEVELOPMENT

I. INTRODUCTION

This is the final report of the first phase of a program whose goal is to place a reliable angle sensor in the NASA National Transonic Facility (NTF). The results of this contract established the optical and electrical parameters required for a system to work under the flow conditions of the NTF and led to a preliminary design for a two-axis laser angle sensor. The body of the report is divided into the following sections.

A. Optical Distortion Measurements - details of optical measurements at the NASA 0.3-m TCT.

B. Window Technology - analytical and experimental information on model window materials for cryogenic use.

C. Two-Axis Breadboard - an optical and electronic breadboard experiment for evaluating different measurement concepts.

D. Preliminary Design - schematics and expected performance specifications of a two-axis laser angle sensor.

The final task of contract NAS 1-15987 was to estimate the cost for design, fabrication, and installation of a laser angle measurement system for the NTF. The documentation for this task is part of a technical proposal submitted to NASA-Langley in June, 1980.

II. OPTICAL DISTORTION MEASUREMENTS

Optical distortion measurements were made with a special shearing interferometer (Figure 1) at the NASA 0.3-m TCT during the period of January 10-16, 1980. Measurement conditions included three pressures (25, 50, and 80 psia), three temperatures (100, 200, and 320°K) and three mach numbers (0.3, 0.6 and maximum mach number). At each test condition, measurements were made for fringe angles of 1/8, 1/4, 1/2, 1, and 2 degrees. (The fringe angle is λ/S, where λ = wavelength and S = shear).

The interferometer was positioned above the test section and a flat mirror was mounted on the floor of the test section. Two optical configurations were used: (1) The interferometer beam was introduced at the forward window, reflected off the mirror, and extracted at the center window to produce a 4-ft optical path in the test section. (2) A cube corner retroreflector was mounted over the center window to fold the beam back to the forward window, producing an 8-ft optical path.

Figure 2 is a top view of the interferometer. The laser beam is recollimated then reflected down to the mirror. The emerging beam is reflected through a 5-position shear plate, the resulting interference fringes are chopped with a code disc, then the modulated signal is focused on a photodetector. The variation of the ac envelope amplitude is measured with a Honeywell type SAI-42A Probability Analyzer.

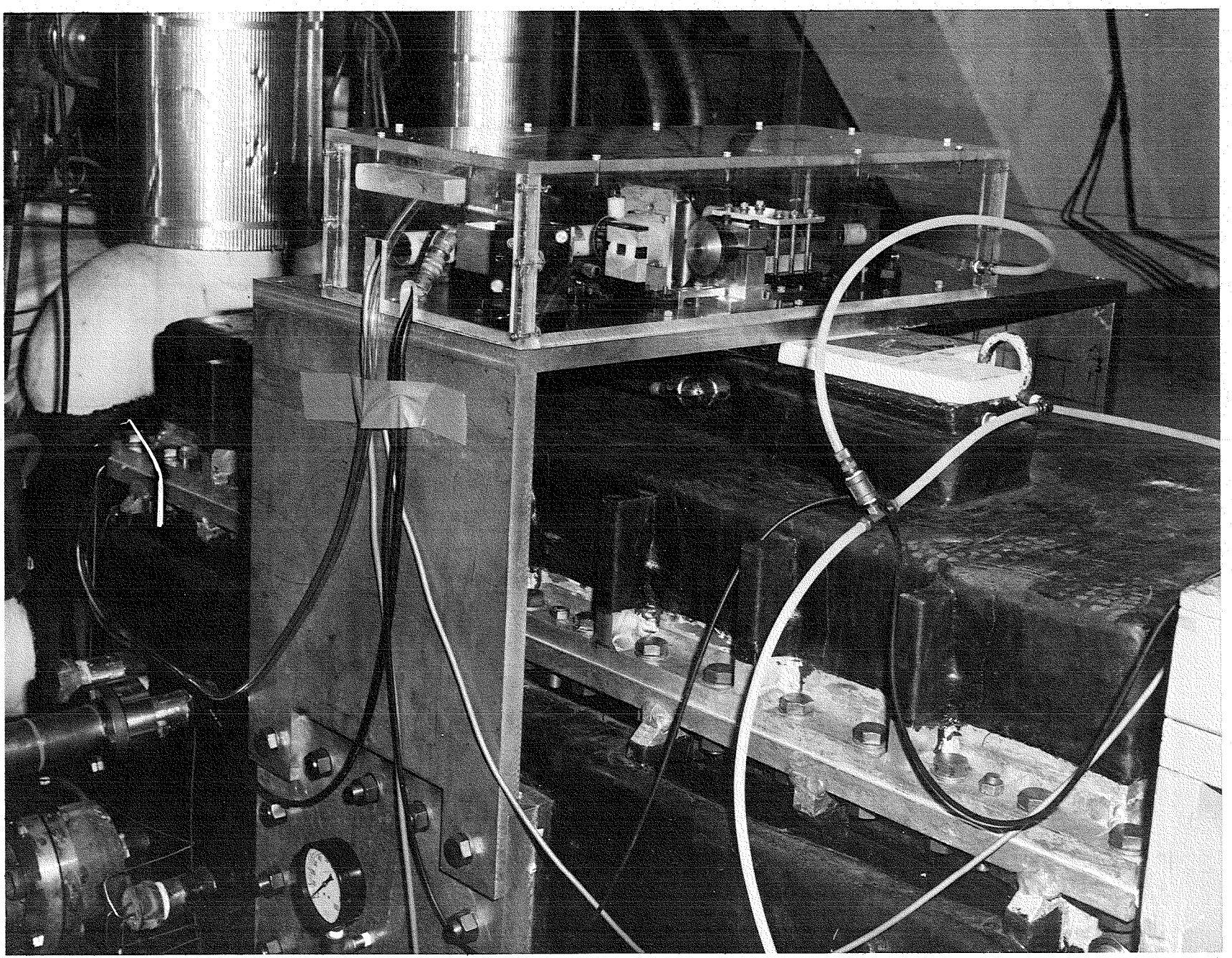

Figure 1: Photograph of the Set-Up at the 0.3-m TCT Flow Test

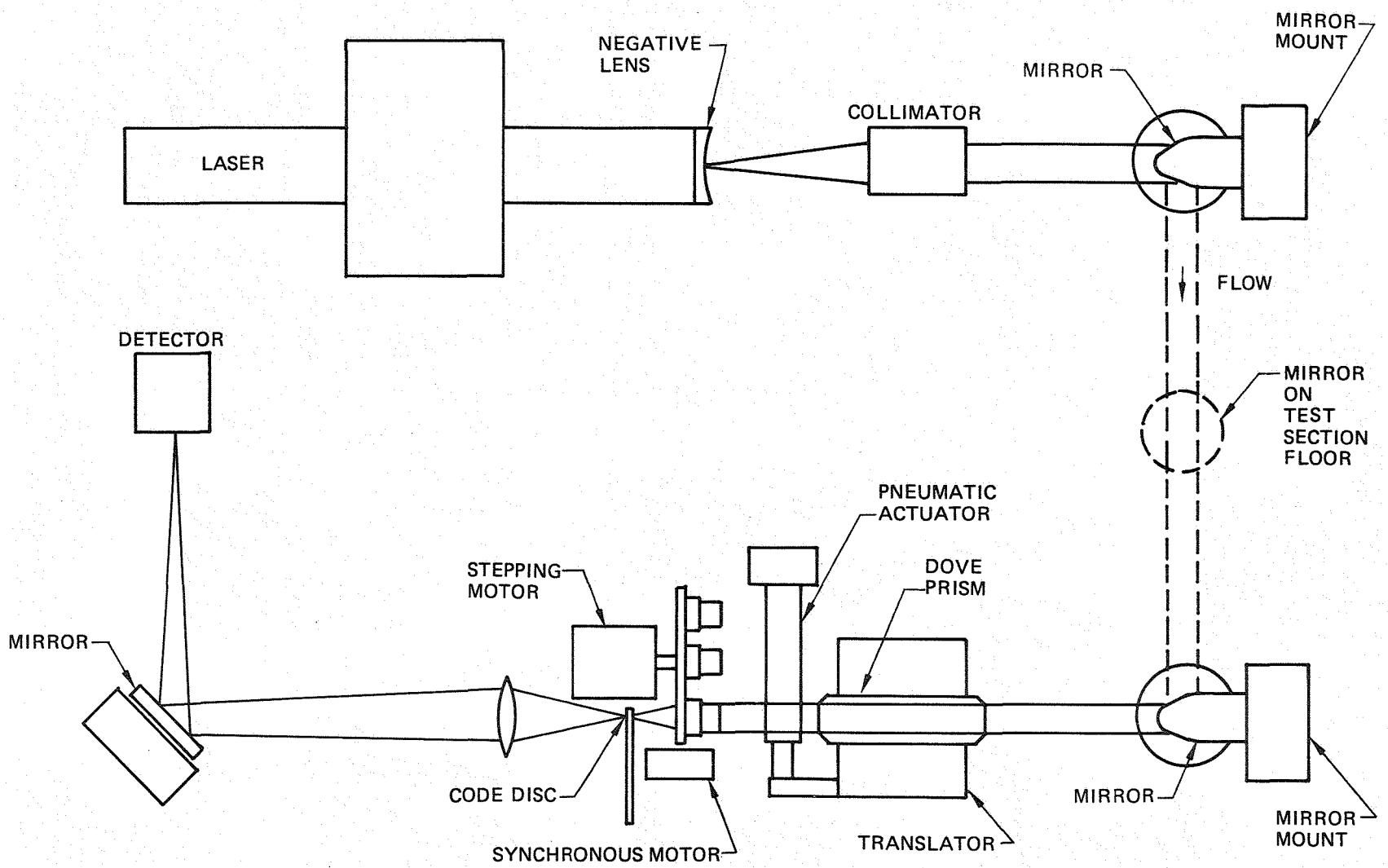

Figure 2: Top View of Optical Distortion Measurement Set-Up (Single Pass Arrangement Shown)

The raw test data consists of a photograph of an oscilliscope trace of the probability analyzer output and a photograph showing the ac waveform with the detected amplitude superimposed on the photo. Typical data is shown in Figure 3. The ac waveform (upper traces) are similar but the detected amplitudes near zero when the fringe angle is 1/4 degree.

Figure 4 is a block diagram of the electronic instrumentation used in the 0.3-m TCT flow tests of January 1980. Figures 5 through 8 are schematics of the electronic circuitry. The light signal is received by a United Detector Technology UDT 450 detector and amplifier in a TO-5 package, followed by a LM365 current amplifier, Figure 5, driving approximately 100 feet of twisted pair shielded wire. Initially, no bandpass filter was used before the envelope detector, Figure 6. To more closely simulate the eventual system configuration, a bandpass filter of $\pm$ 1KHz, Figure 7 was used before the wideband envelope detector. The envelope detector is followed by three 4 pole low pass filters, Figure 8, with cut off frequencies of 500 Hz, 2000 Hz, and 5000 Hz.

The probability density data (Figure 3) is a measure of the mutual spatial coherence of the two sheared beams. The ac envelope goes to zero when the fringes are washed out due to density variations in the flow. At a given flow condition, the fluctuations in the ac envelope increase as the fringe angle decreases. At some minimum fringe angle the envelope goes to zero at times and defines the extreme operational limit for an integrating laser angle sensor. Any system with a smaller fringe angle accumulates errors if the model angle changes while the ac envelope is near zero.

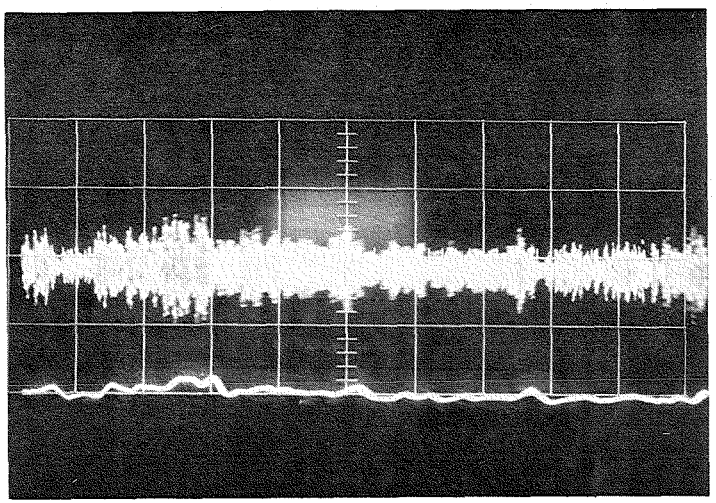

FRINGE ANGLE = 0.25 DEGREES

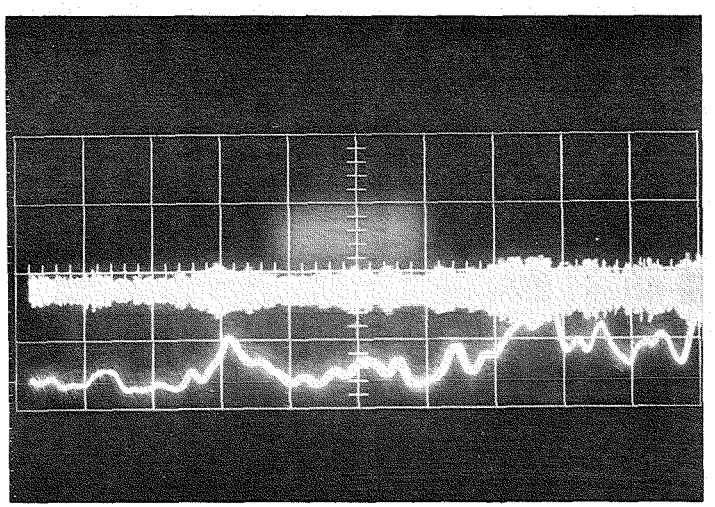

FRINGE ANGLE = 1 DEGREE

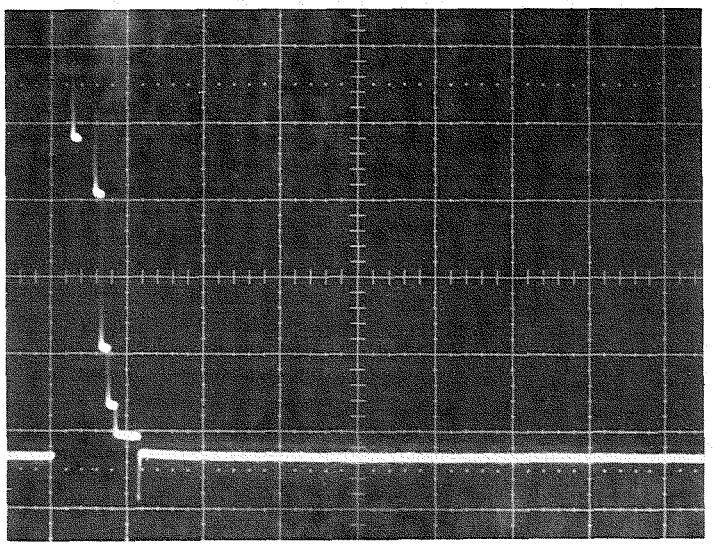

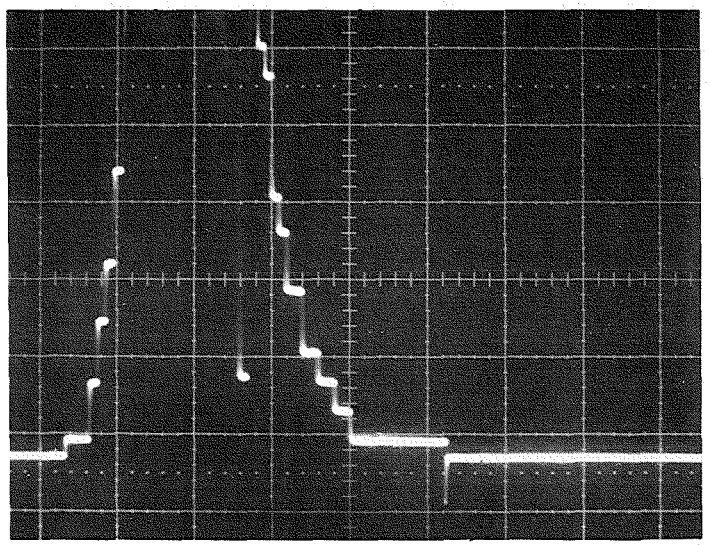

Figure 3: Double Pass Optical Distortion Measurement at 100°K, 80psi and Mach No. = 0.7, Raw Data and Detected Amplitude on Upper Photos, Corresponding Probability Density on Lower Photos.

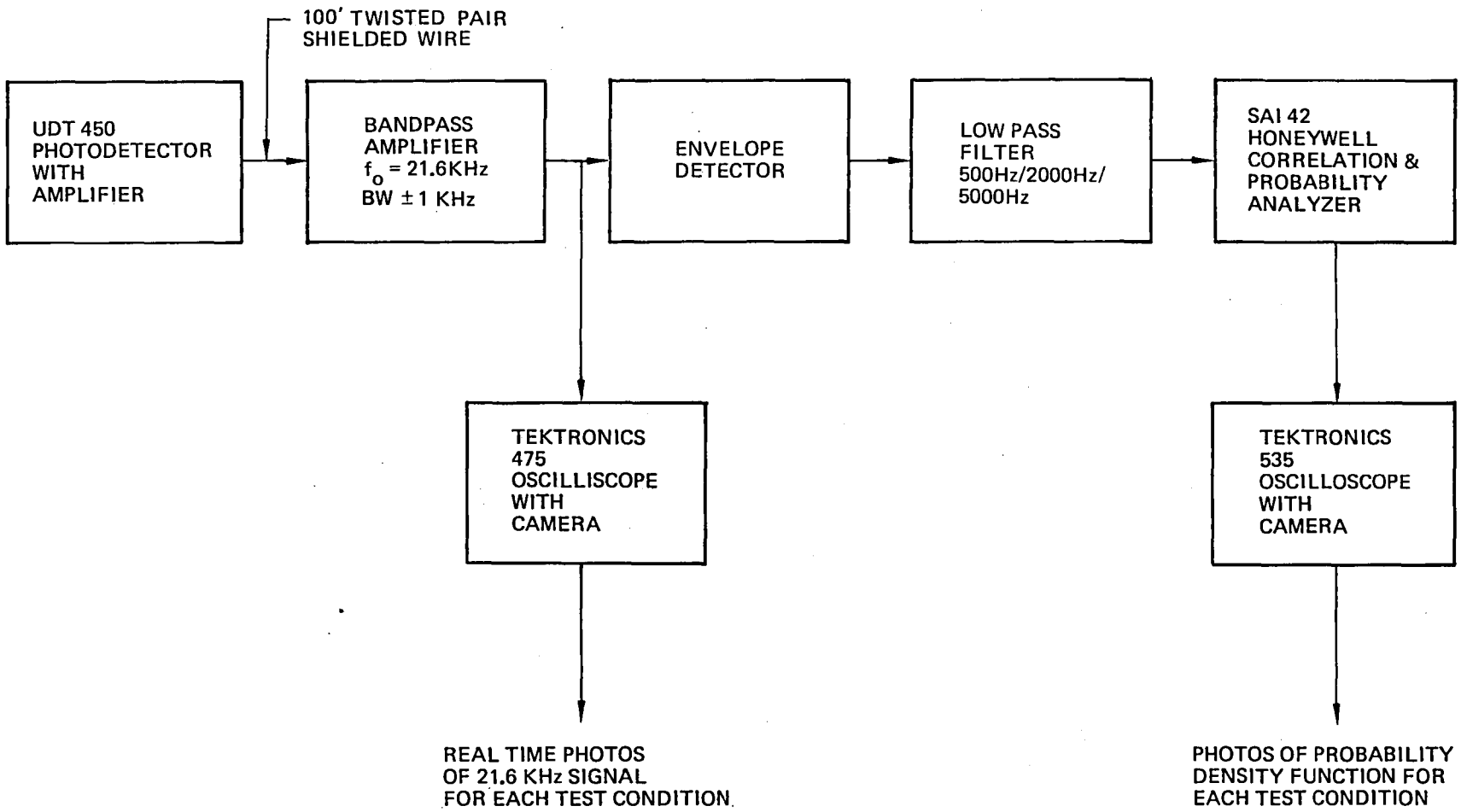

Figure 4: Instrumentation Block Diagram for Cross & With Flow Tests Jan. 1980

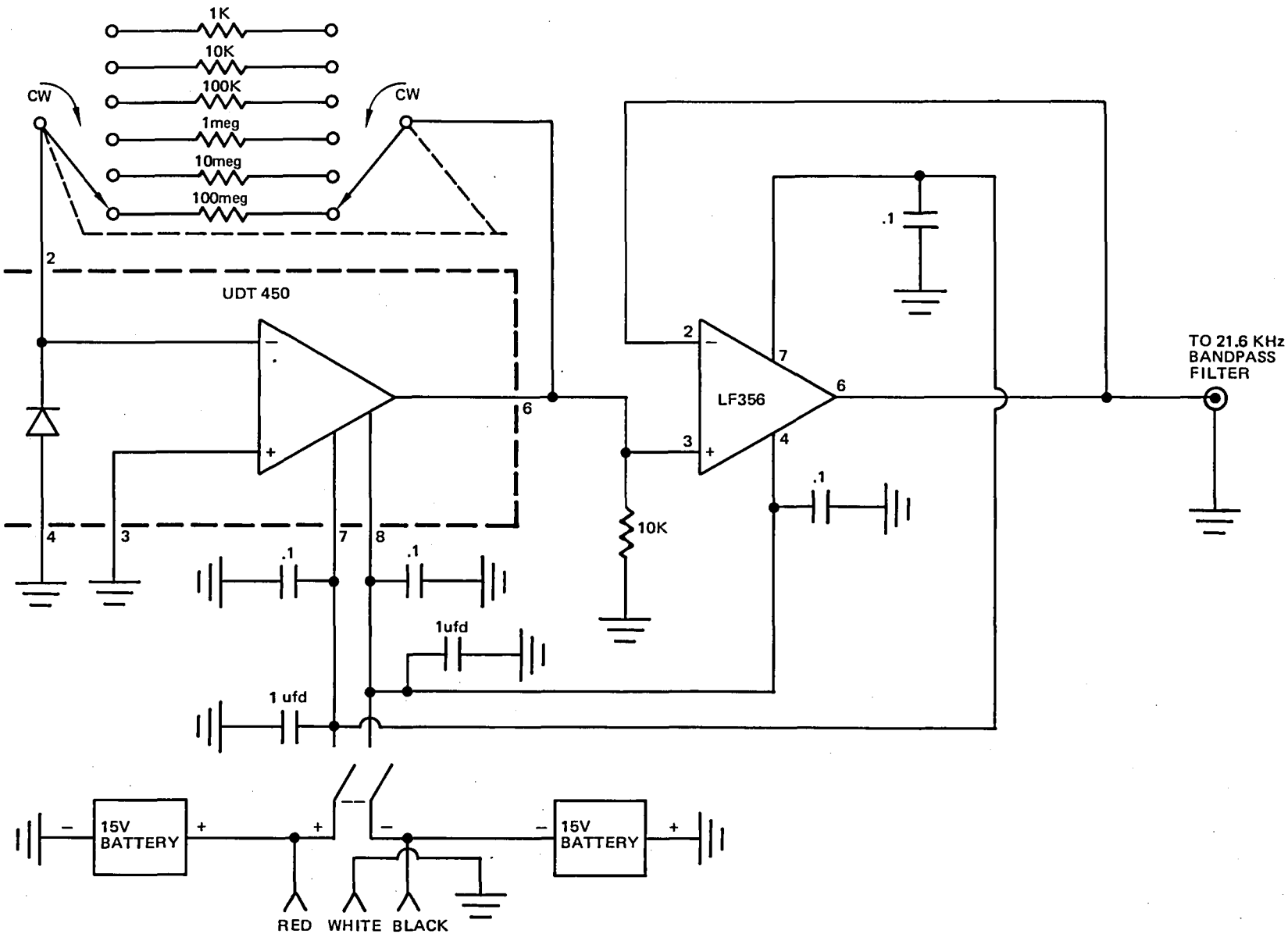

Figure 5: Photodetector Circuit for Langley 0.3-m TCT Flow Test

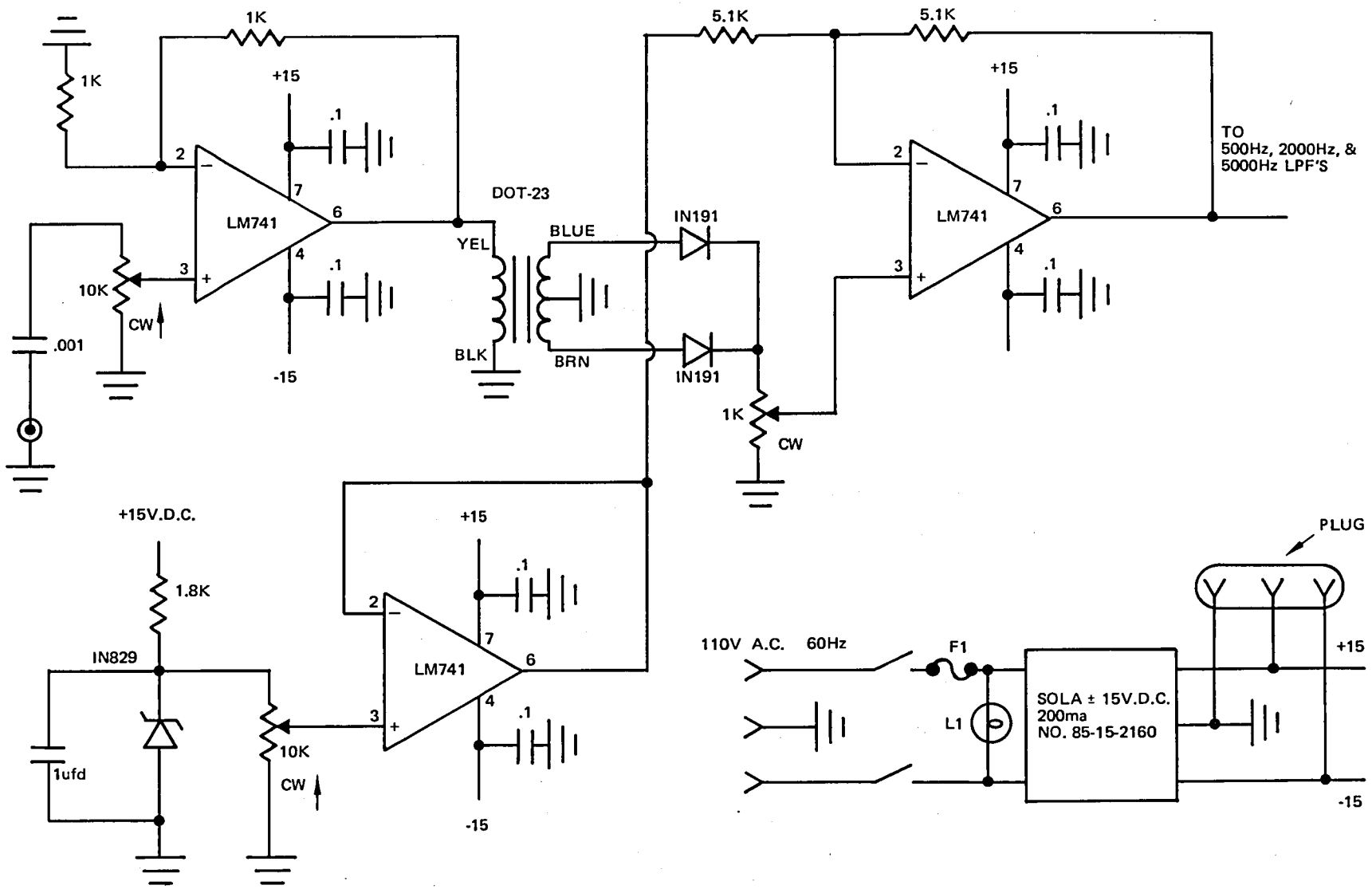

Figure 6: Envelope Detector for Langley 0.3-m TCT Flow Test

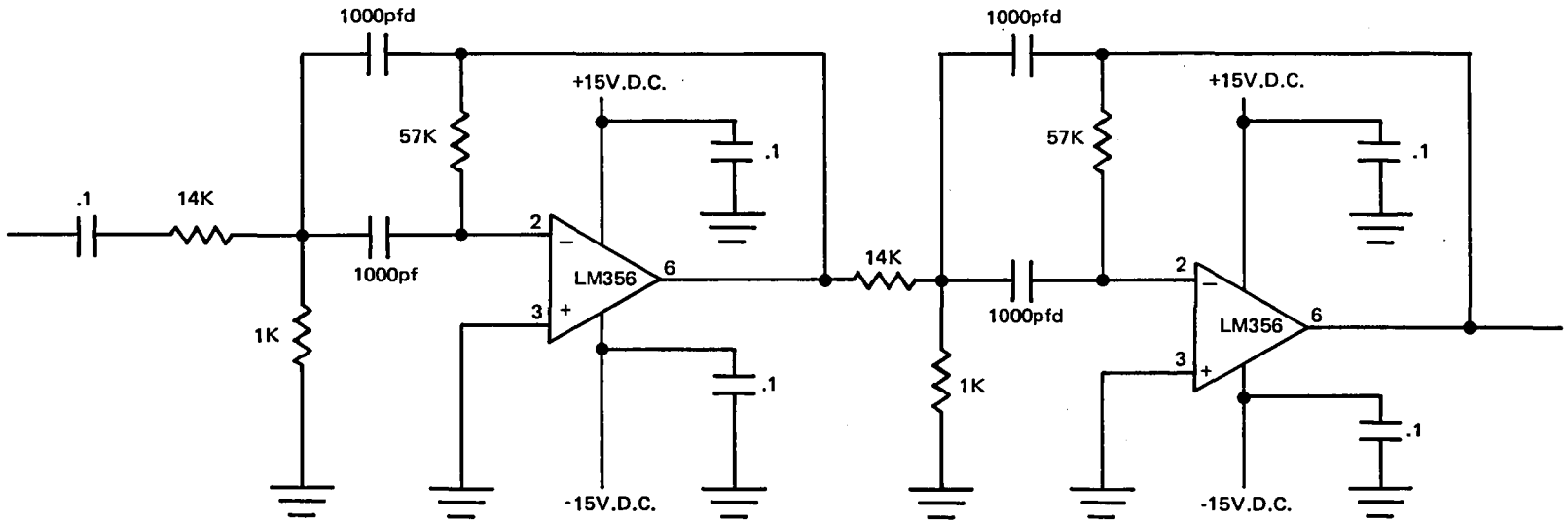

fo = 21.6KHz
BW = ± 1KHz
A ≅ 4

Figure 7: Bandpass Amplifier for Langley 0.3-m TCT Flow Test

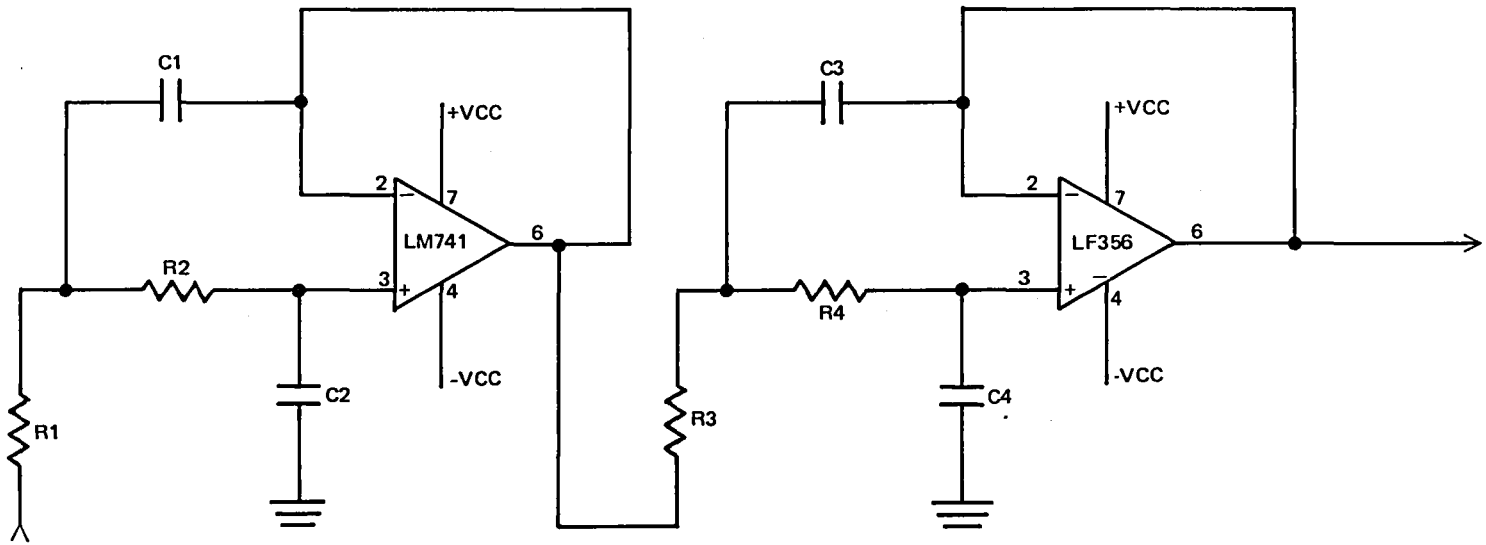

fc = 500Hz		fc = 2000Hz		fc = 5000Hz	
C1	.1	C1	.1	C1	.1
C2	.01	C2	.01	C2	.01
C3	.1	C3	.1	C3	.1
C4	.047	C4	.047	C4	.047
R1	19.035K	R1	4.759K	R1	1.904K
R2	5.316K	R2	1.329K	R2	531
R3	9.675K	R3	2.419K	R3	968
R4	2.1K	R4	525	R4	210

NOTE: USE RESISTANCE VALUES AS CLOSE TO VALUES SHOWN

Figure 8: 4 Pole Low Pass Filters for Langley 0.3-m TCT Flow Test

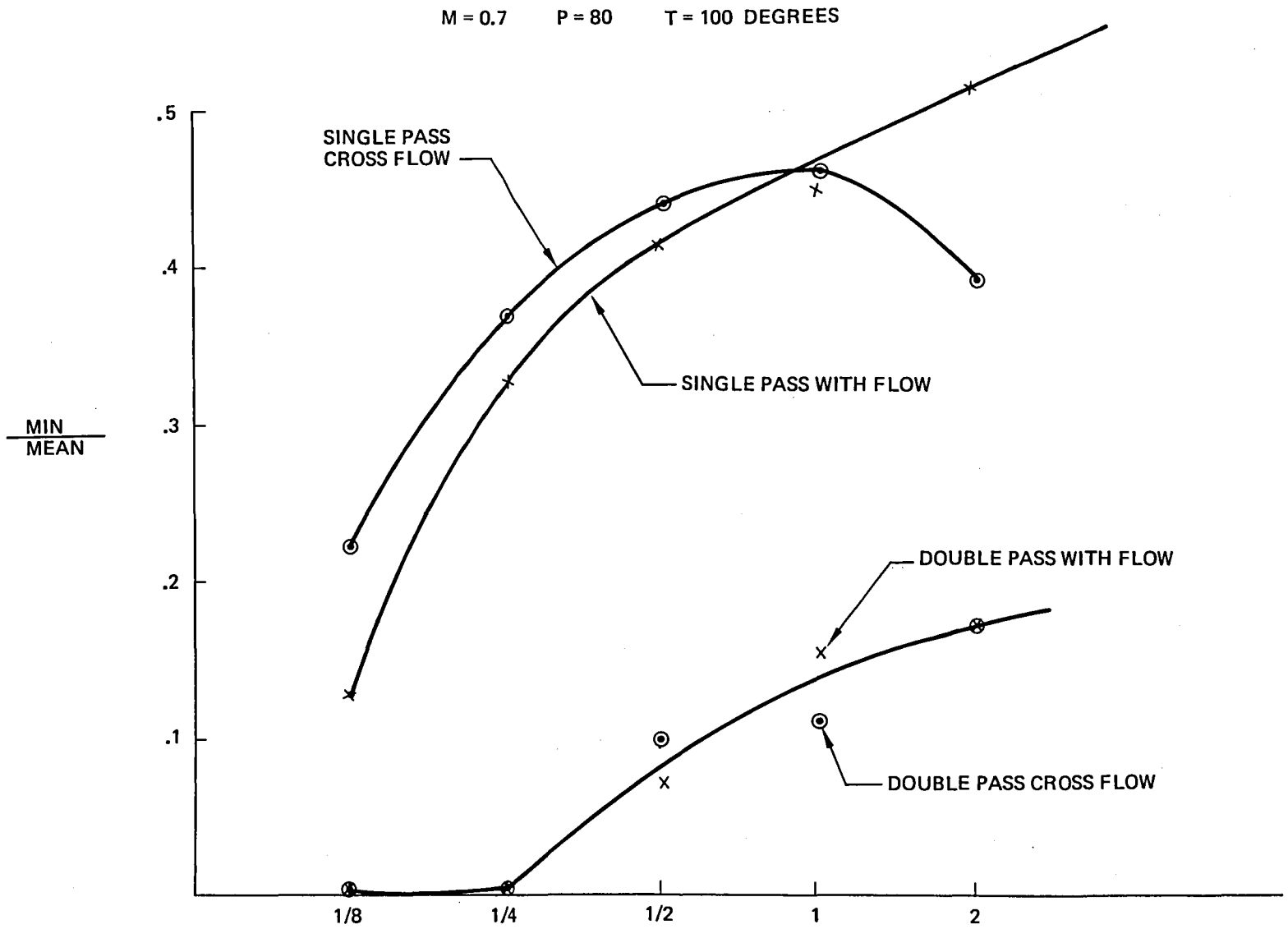

Figure 9: Probability Density $\frac{min}{mean}$ vs. Angle

In order to compare the probability density data in a way that is relevant to the performance of a laser angle sensor, the ratio of the minimum to the mean value was plotted as a function of fringe angle (Figure 9). At the extreme test condition (M = .7, P = 80, T = 100) the single pass data shows a drop between $1/4^{o}$ and $1/8^{o}$. The double pass data drops to zero below $1/2^{o}$. The single pass data simulates the 4-ft optical path between the laser and the model in the NTF at the above test condition. (Note that it is only the optical distortion from the laser to the model that is important, as the interference fringes are generated by the reflector assembly on the model. Optical distortion in the return path does not cause amplitude modulation in the signal.) The double pass data simulates the optical conditions that can be anticipated for a high pressure condition of the NTF, since the total mass of nitrogen gas in the optical paths are comparable.

The optical distortion measurements underscored one potential problem with an integrating laser angle sensor of the type built under contract NAS1-15410. There were many times during the test when the nitrogen "fog" was so thick that the signal was near zero. Discussions with NASA personnel indicate that this may occassionally happen in normal operation of the NTF, as there will be a desire to operate the tunnel at the lowest possible temperature in order to achieve maximum Reynolds number. Nitrogen fog may be produced intermittently as the flow approaches test conditions. (Note that continuous fog in the test section cannot be tolerated, as it is necessary to monitor the model dynamics on a closed-circuit television.)

An integrating laser angle sensor counts fringes from a known zero-alpha position. If the signal drops out due to fog, an error in the fringe count may be produced if the model angle is changing. The angle reading may be reset to zero after bringing the model back to zero, but this increases the run time. A non-integrating laser angle sensor that measures the absolute angle would save time during conditions of intermittent fog.

The optical distortion measurements demonstrated that interferometric angle measurement techniques can work at high pressure and cryogenic temperature. The fringe angle should be at least 0.5 degrees. Optical distortion can produce signal dropouts if the fringe angle is 0.25 degrees or less. Some provision for resetting the angle after nitrogen fog conditions in the flow will be required.

III. WINDOW TECHNOLOGY

The model windows must protect the reflector assembly and provide a smooth transition from the model to the window. Optical distortion due to window curvature must be small compared to the fringe angle. Temperature changes from room temperature to 77°K restricts the range of possible window materials and necessitates special care in mounting the window. Finally, the window and mount must be designed so that fabrication costs are low.

One of the major considerations in selecting the window material is the difference in thermal expansion between the window and the model. If the coefficient of thermal expansion of the window is greater than the model, a gap may open up at the edge of the window as the model cools down. On the other hand, if a low expansion window is used (fused silica for example), model contraction can produce high stresses in the window. In addition, the edge of the cold window may rise above the contour of the model, producing a step that disrupts the flow over the model.

A computer program was written to calculate the thermal stress in a window due to rapid cooling. The calculation assumes a step increment in the temperature of one side of the window. Figure 10 shows the results of a calculation for a 2.54 cm disc of BK-7 glass with a thickness of 3 mm. This example can be used to estimate the stresses for other glasses and other temperature limits, since the stress is proportional to both the expansion coefficient and the temperature difference. Note that the calculated case is an extreme condition that will not happen in practice, since the surface cannot be cooled in zero time.

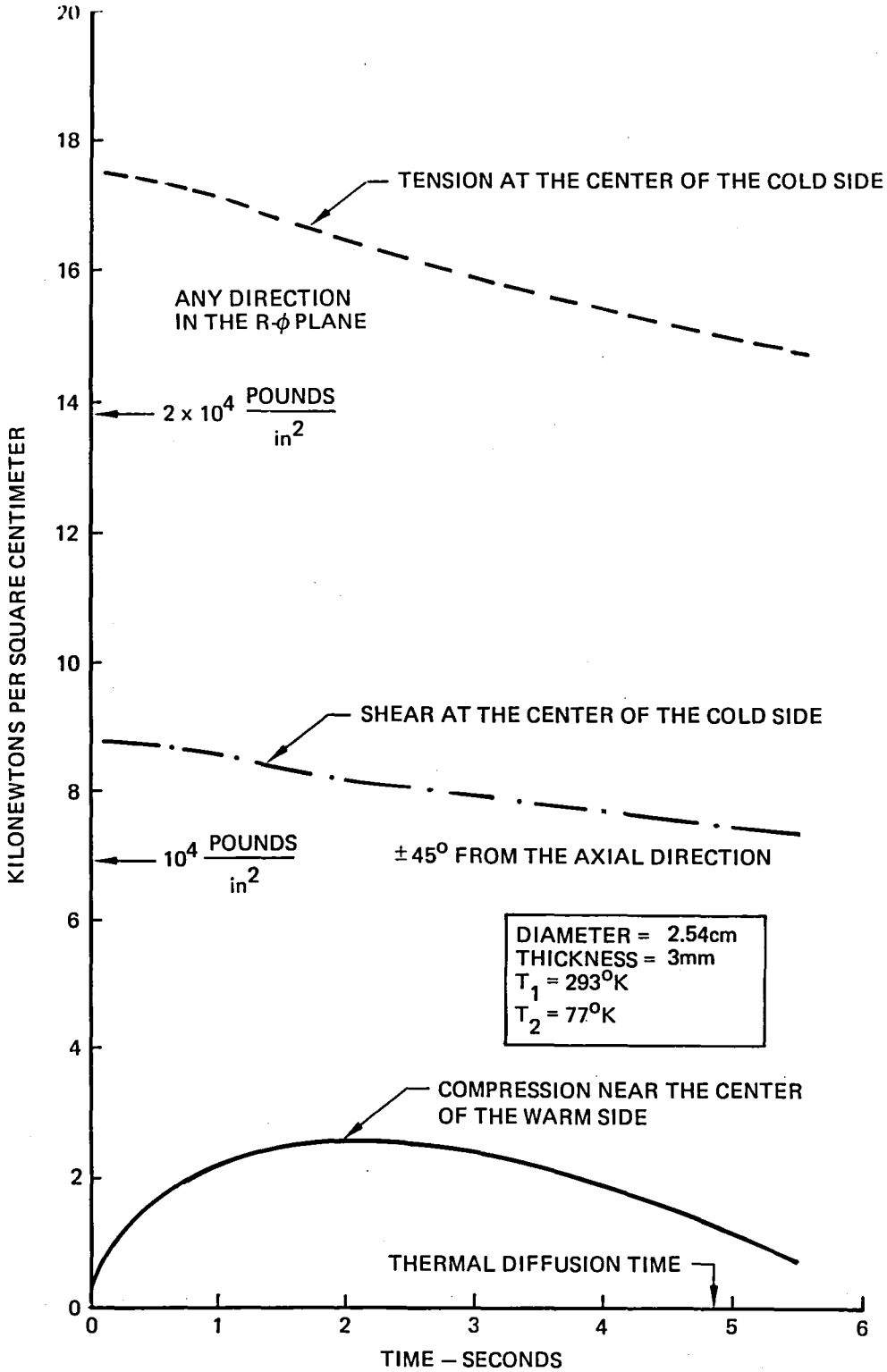

Figure 10: Thermal Stresses On a BK-7 Glass Disk

There is always a boundary layer that limits the transfer of heat across the surface.

Several glass plates (1 mm to 6 mm thick) were tested for thermal shock failure by direct cooling with liquid nitrogen on one face. There was no damage to specimens in good condition. However, each specimen was then scratched with a diamond tool and the test was repeated. One 6 mm thick specimen failed during the first cooling cycle, while a second 6 mm thick specimen, a 3 mm thick chemically tempered specimen and a 1 mm specimen showed no crack growth after several cycles. It appears that the boundary layer will protect the window from thermal shock failure.

In addition to the thermal characteristics, the window must withstand pressure loading. The required thickness to diameter ratio for an unclamped circular window with a safety factor of 4 is:

$$\frac{t}{D} = 1.06\sqrt{\frac{P}{F_a}}\text{ , where}$$

t = thickness

D = diameter

P = pressure difference

F_a = apparent tensile failure stress

If P = 130 psi and F_a = 10,000 psi, then t/D = 0.121. The thickness must be at least 0.060-in. if the window diameter is 0.5-in.

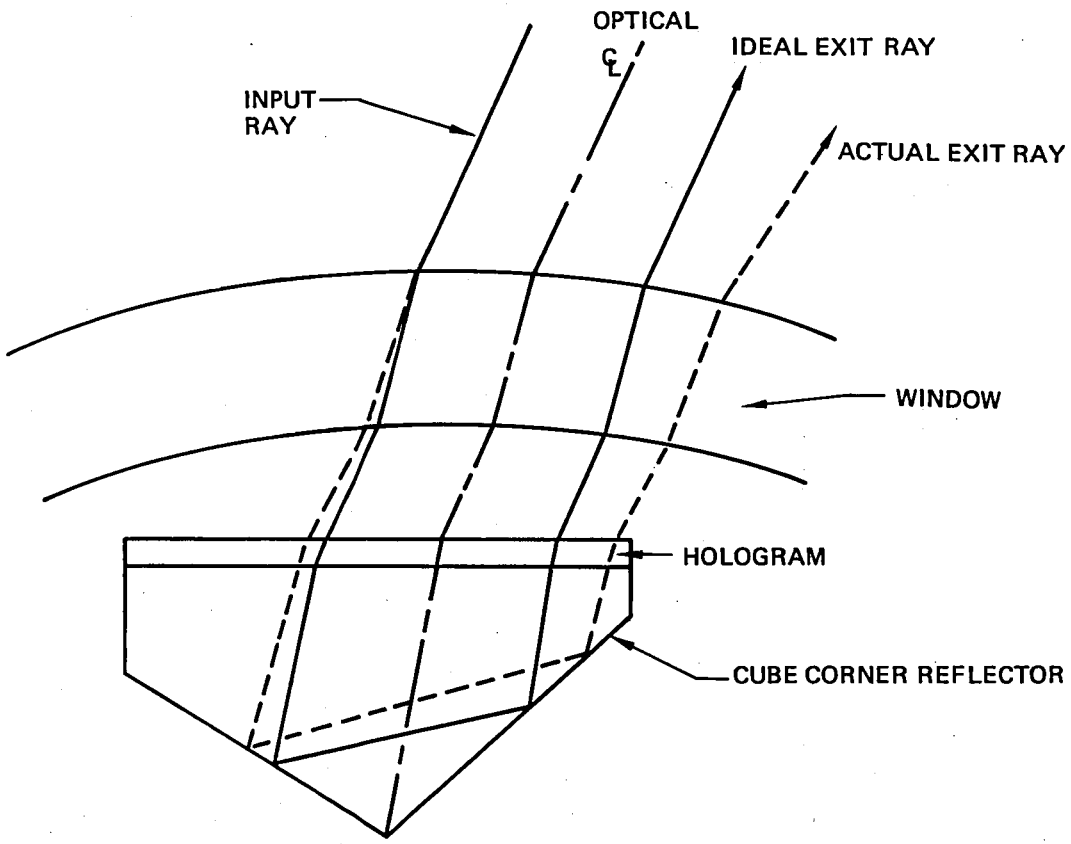

Figure 11: Optical Distortion Due to Window

The breaking stress can actually increase at cryogenic temperatures. Table 1 (from "Cryogenic Engineering," R. B. Scott, D. Van Nostrand, Inc., 1959, p. 327) shows the breaking stress of abraded and unabraded glass specimens when subjected to changing loading conditions. The breaking stress of all of the specimens increases as the temperature decreases, and the glass also becomes more resistent to failure from long term stress.

TABLE 1 - BREAKING STRESS OF A BOROSILICATE GLASS (BSC-2, CORNING 8370)

Condition	Rate of Stress Increase $lb\text{-}in^{-2}\text{-}sec^{-1}$	Breaking Stress, $lb\text{-}in^{-2}$			
		296°K	194°K	76°K	20°K
Abraded	800	7500	9500	10,400	10,400
Abraded	10	5500	7500	10,400	10,600
Abraded	1	5000	6400	10,400	10,200
Unabraded	800	10,400		18,000	

The reflector assembly is usually mounted on the body of the model, where the contour is approximately cylindrical. The window acts as a cylindrical lens. Since the axis of the cylinder is parallel to the body axis, the return beam is spread out in the cross-flow direction. Figure 11 is a view looking along the body axis that shows the deviation of the return beam due to refraction at the cylindrical surfaces.

A computer program was developed to trace the rays through the window. The results of a particular case are shown in Table 2 below, where the angular deviation is in the roll direction. The effect of the beam deviation is to reduce the modulation index of the return signal beam. The modulation index is zero when total deviation equals the fringe angle.

TABLE 2 - BEAM DEVIATION THROUGH A CYLINDRICAL WINDOW

Distance from optical centerline (millimeters)	0.5	1	1.5	2	2.5	3
Angular deviation (degrees)	.032	.064	.096	.128	.160	.193

Window geometry used in the calculation:

Outer radius = 50 mm

Inner radius = 47 mm

Thickness = 3 mm

Index of refraction = 1.5

Angle of attack = 20^{o}

Roll angle = 20^{o}

Figure 12 shows several possible techniques for mounting the window. A window fused to a glass cylinder (Figure 12-b) was fabricated during the study to demonstrate the feasibility of this technique. The metal/glass seal technique (Figure 12-c) is quite common, and is used in the construction of some flashlamps. However, the mechanical technique shown in Figure 12-a is preferred because of simplicity.

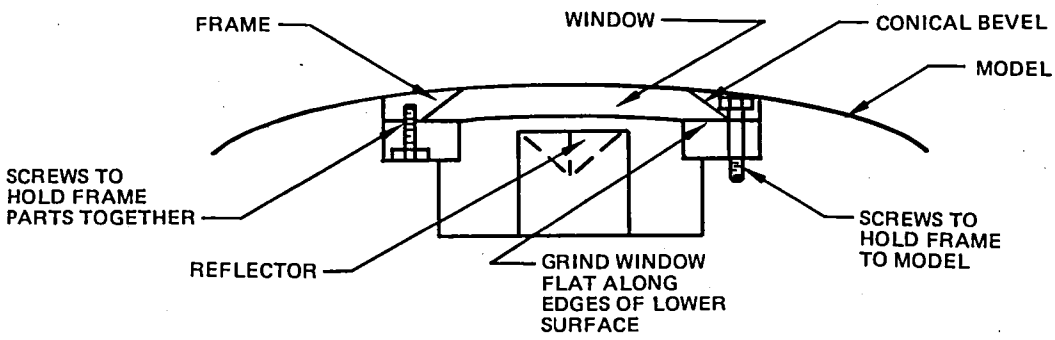

(a) Mechanical

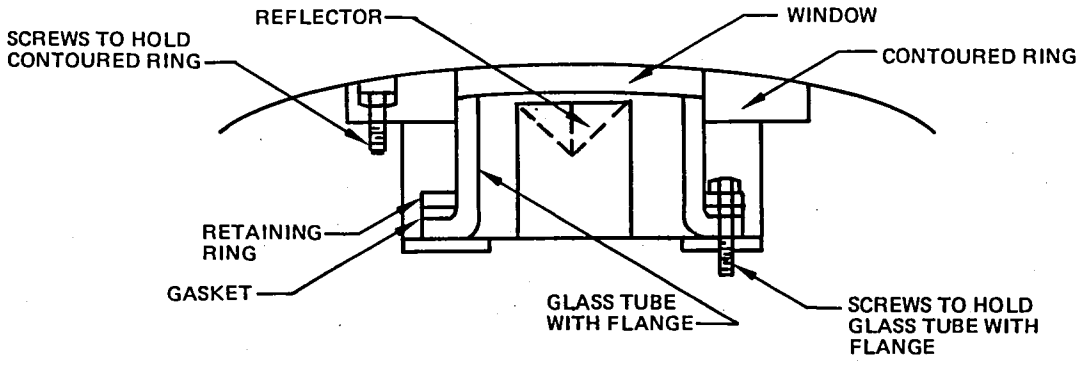

(b) Window Fused to Glass Cylinder

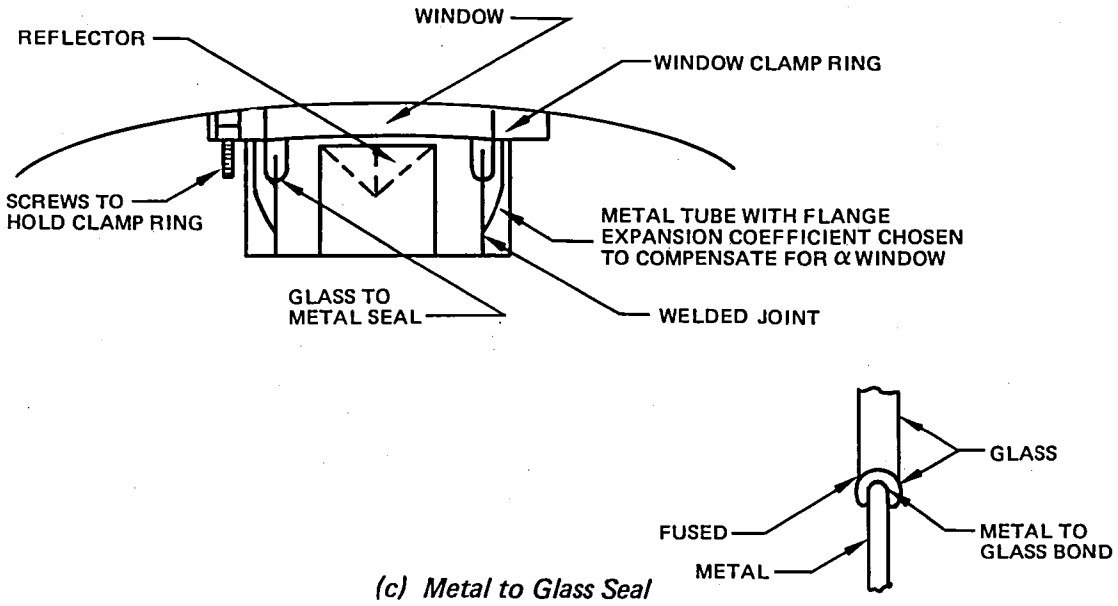

(c) Metal to Glass Seal

Figure 12: Window Mounting Techniques

IV. TWO-AXIS BREADBOARD

A two-axis breadboard was assembled for experimental evaluation of a pitch/roll angle measurement system. Several optical configurations were used, and three electronic processing methods were compared.

Figure 13 shows the basic optical configuration. Figures 14 and 15 are photographs of the breadboard setup. The laser is a 4 milliwatt helium-neon laser (λ = 633 nm). The beam is split into two beams with a beam splitter. A negative lens and a cylindrical lens near the laser exit aperture form the beams into line shaped spots (0.3x2-cm) at the plane of a 36-element multiple lens disc. The spots are spaced 90^{o} apart at the lens disc, with the 2-cm dimension perpendicular to the disc radius. The lens disc is rotated at 3,600 RPM with a synchronous motor (not shown).

The lens disc produces two linearly scanned optical sources, oriented in the horizontal and vertical directions. The sources are translated toward the disc center with an orthogonal pair of rhomboidal prisms in order to produce a more compact pattern, thereby reducing the overall beam spread from the collimating lens.

One of the major problems with a 2-axis angle measurement system is coupling between the pitch and roll axes. Two methods were used to minimize coupling in the breadboard optics: (1) The pitch and roll beams are spatially separated at the focal plane of the collimating lens; and (2) the beams have orthogonal polarization. The beam geometry is shown in Figure 16. Figure 16-a shows the linearly scanned sources at the focal plane of the collimating lens. The laser

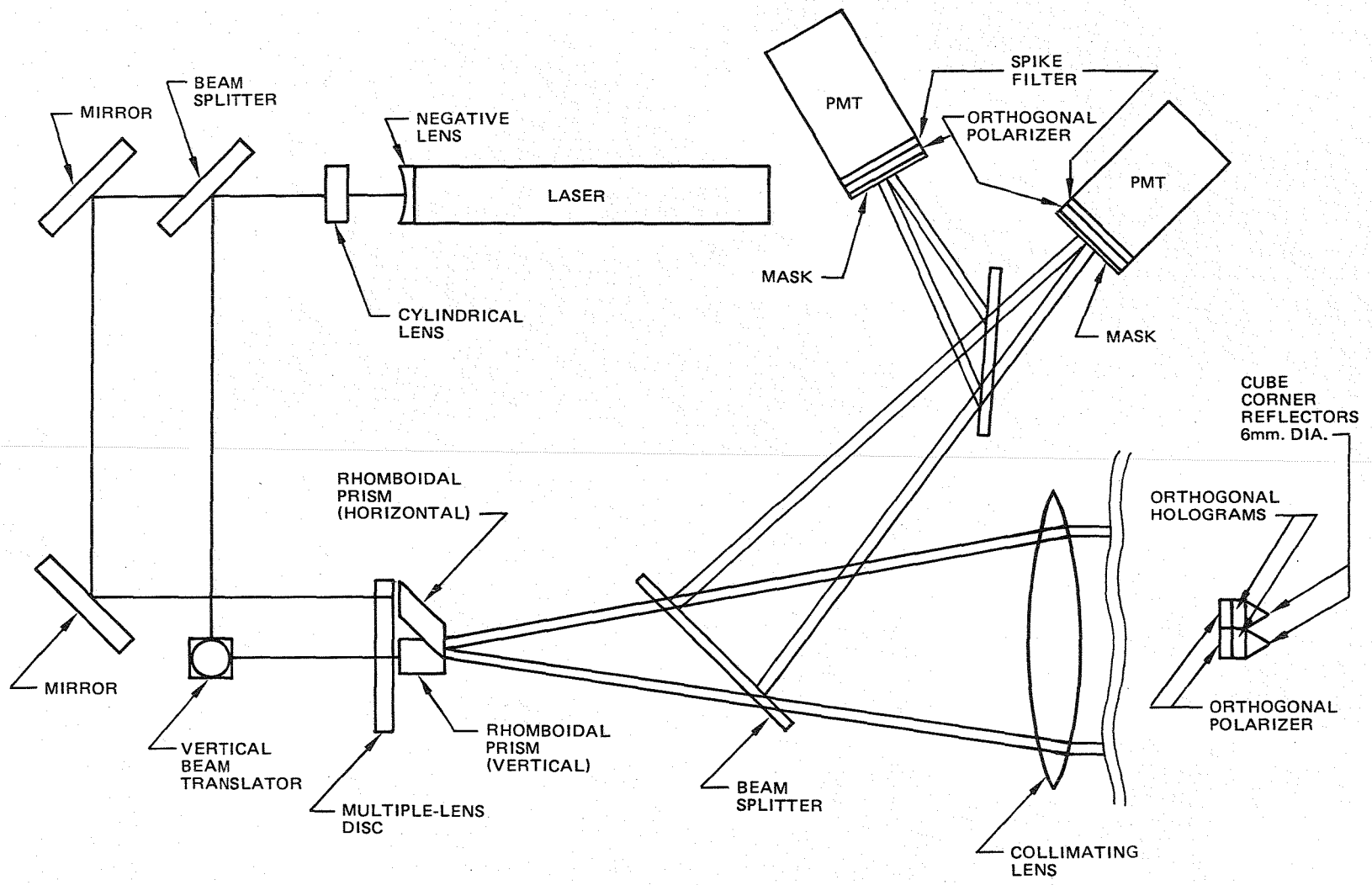

Figure 13: Two-Axis Breadboard Optics

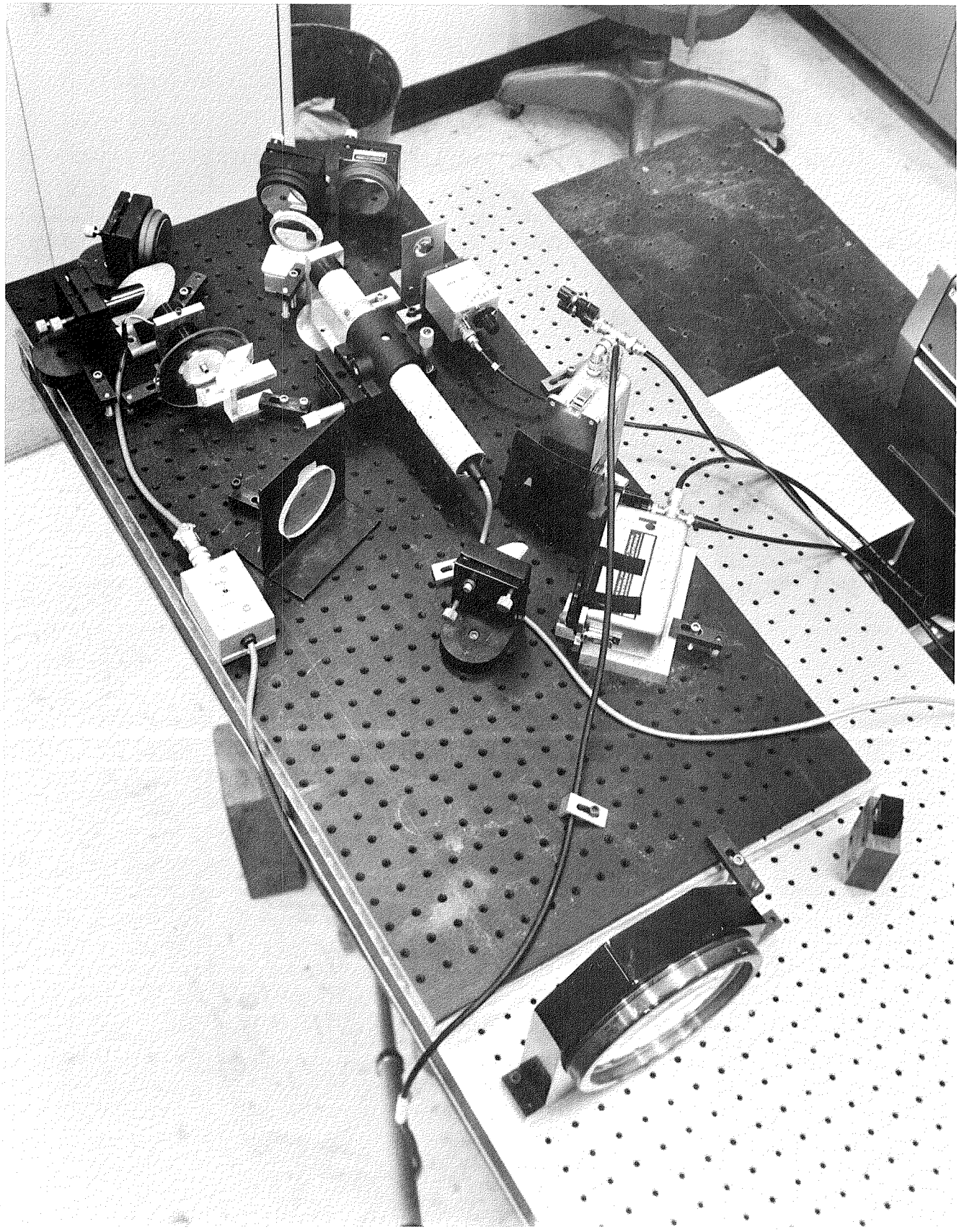

Figure 14: Breadboard Optics

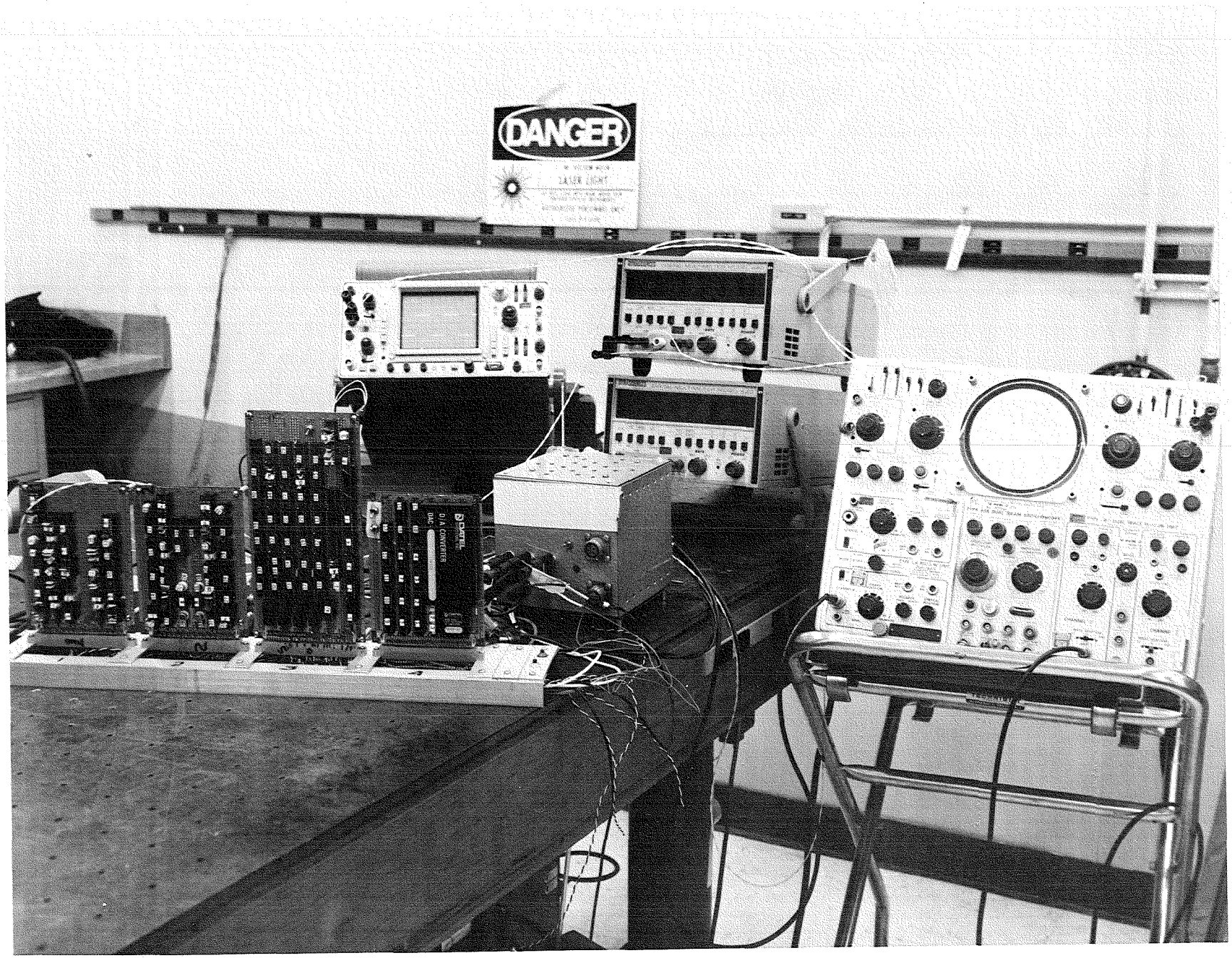

Figure 15a: Breadboard Electronics

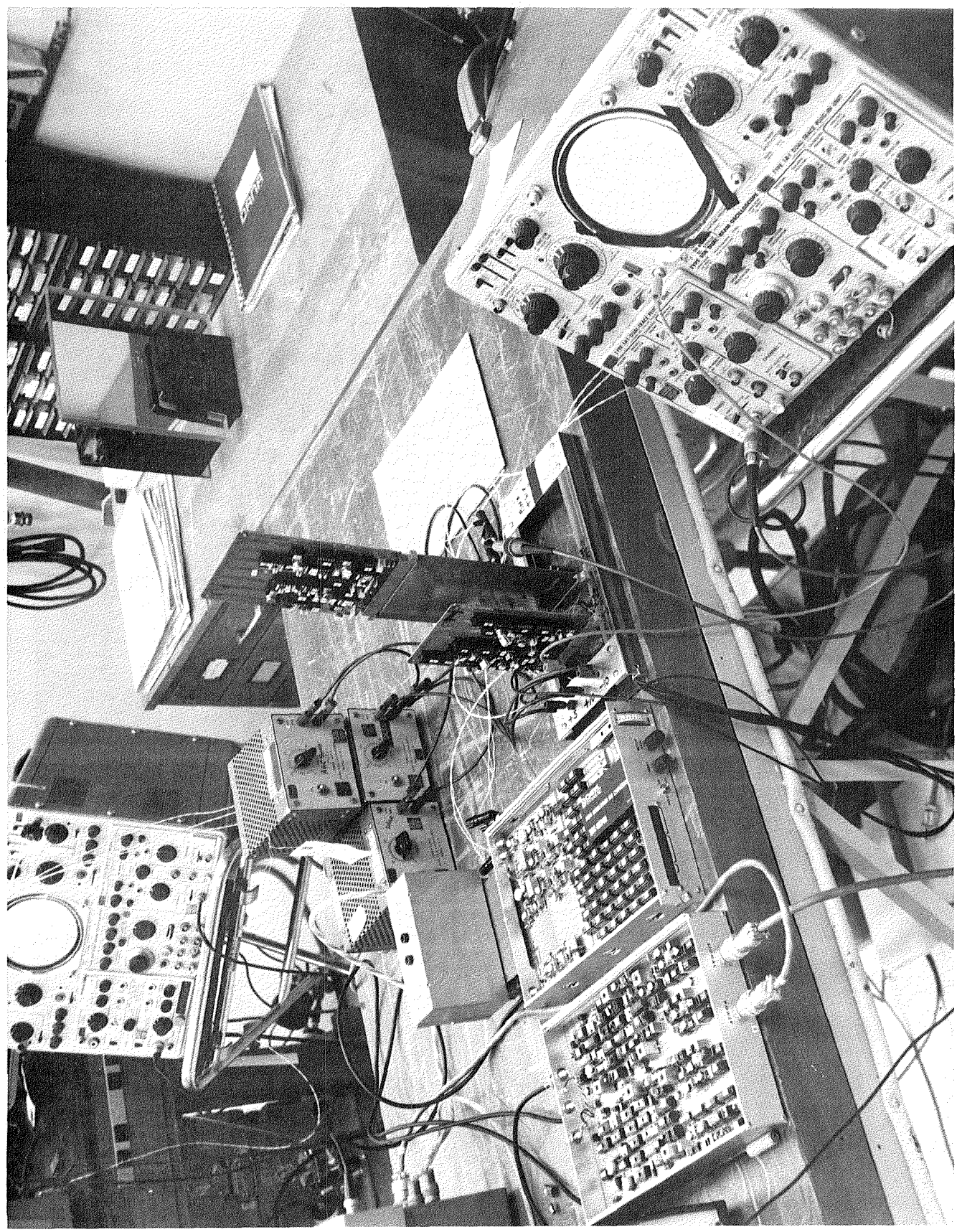

Figure 15b: Breadboard Electronics

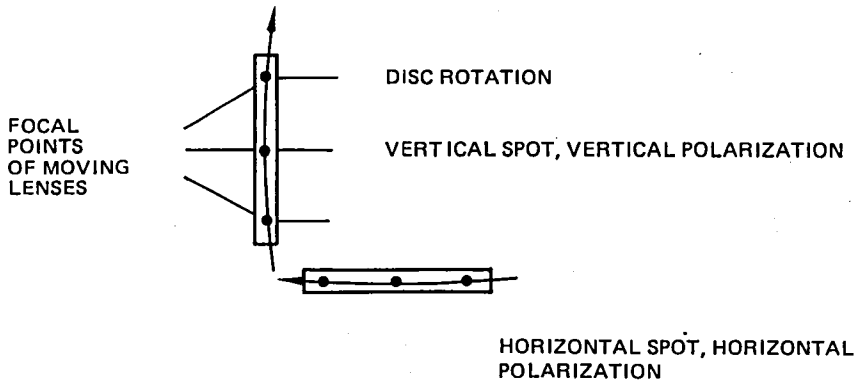

(a) LINEARLY SCANNED SOURCES AT FOCAL PLANE OF COLLIMATING LENS

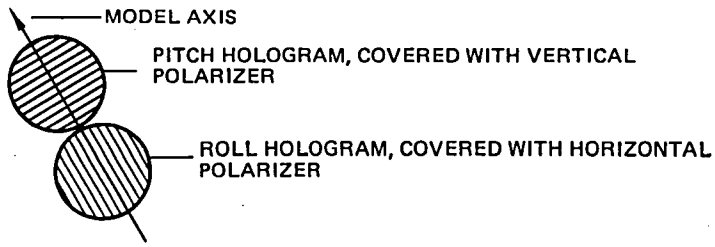

(b) HOLOGRAM ORIENTATION AT REFLECTOR ASSEMBLY

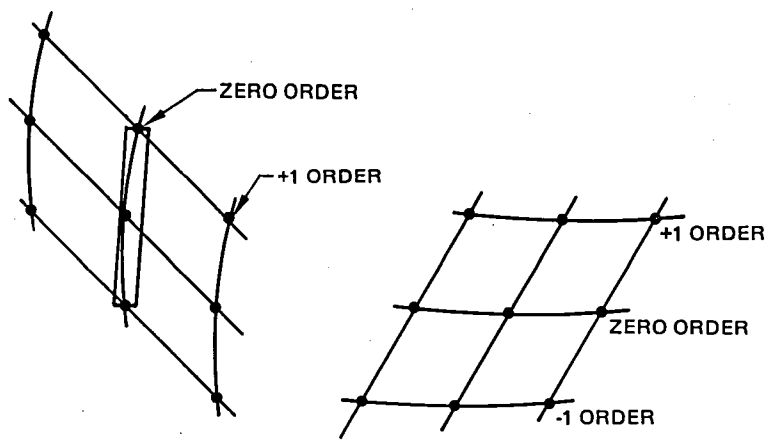

(c) RETURNS BEAMS AT PITCH AND ROLL DETECTORS

Figure 16: Details of Pitch/Roll Beam Geometry

is polarized in the vertical plane, so the vertical source is also polarized in this direction. The vertical beam translator rotates the plane of polarization 90^{o}, so the horizontal source has horizontal polarization.

The model axis is inclined at 45^{o} relative to the breadboard optics, as shown in Figure 16-b. The grating orientation in the pitch (roll) hologram is perpendicular (parallel) to the model axis, producing return spots arranged as shown in Figure 16-c. A mask at the detector entrance aperture selects either the -1, 0, or +1 diffraction order. Both zero and first orders were used during the evaluation. The best results were obtained using the -1 order beams, where the spatial separation is best. In addition to the basic setup, the breadboard optics were used to evaluate several different techniques, including the following:

(1) The system was used in a single axis mode, with the hologram oriented perpendicular to the scan-direction. The zero order return beam passed back through the lens disc. The signal was detected with a UDT-450 detector behind the first beam splitter. The major problem with this arrangement is that light scattered from the lens disc mixes with signal light producing small scale nonlinearity in the angle measurement.

(2) An infrared diode laser was substituted for the helium-neon laser (single axis mode). The signal characteristics were good, but alignment is difficult.

The required angular resolution of the laser angle sensor is obtained by dividing the fringe angle into an integral number of parts. This is the function of the electronics. Three methods for doing this were evaluated with the breadboard system. These are described in the following order:

(1) Quadrature and multiple quadrature detection

(2) Phase multiplication with quadrature detection, and

(3) Start and stop counter phase measurement.

Since the angular change of the model is bi-directional, quadrature detection is used to determine the direction of the phase change. Figure 17 is a block diagram of a quadrature detector. A reference phase must be generated for processing of the phase modulated signal. The phase modulated signal is applied to two separate phase detectors (balanced modulators were used) and the reference is applied to one directly and shifted in phase by $\frac{\pi}{2}$ radians before it is applied to the other. The output from the phase detector is a voltage proportional to the amplitude of the signal and the cosine of the phase angle between the signal and reference for the respective phase detector. Since phase information is preserved in frequency translation, the output from the two phase detectors are in phase quadrature. The low pass filters remove the undesired products from the outputs of the phase detectors and the analog-to-digital shaper changes the analog signal to a digital signal before application to the direction determining logic.

Figure 18 is a representation of the transfer function for the two phase detectors referenced to an arbitrary zero phase condition. The digital logic representation is also shown. Note that a repetitive sequence exists. The direc-

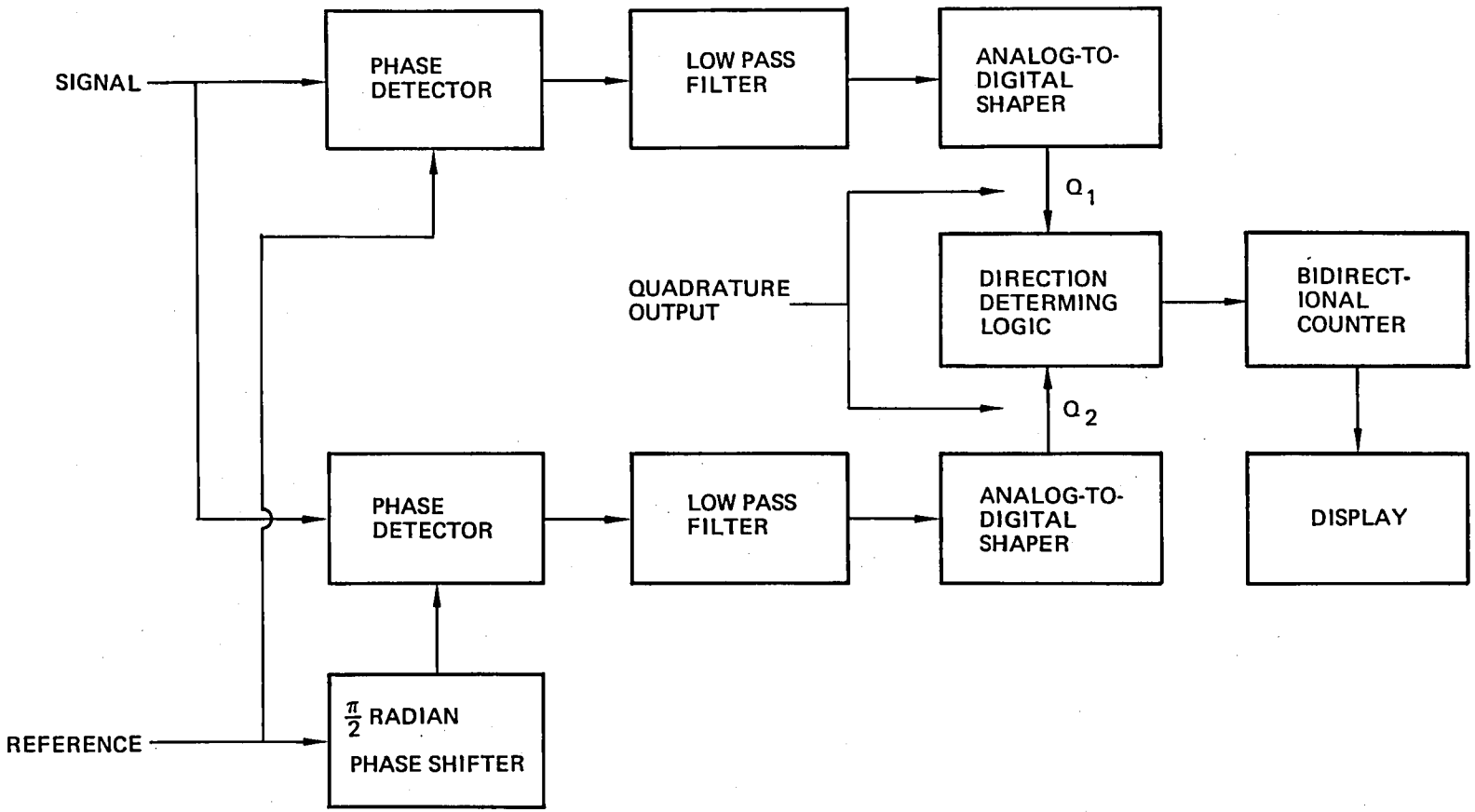

Figure 17: Quadrature Detection

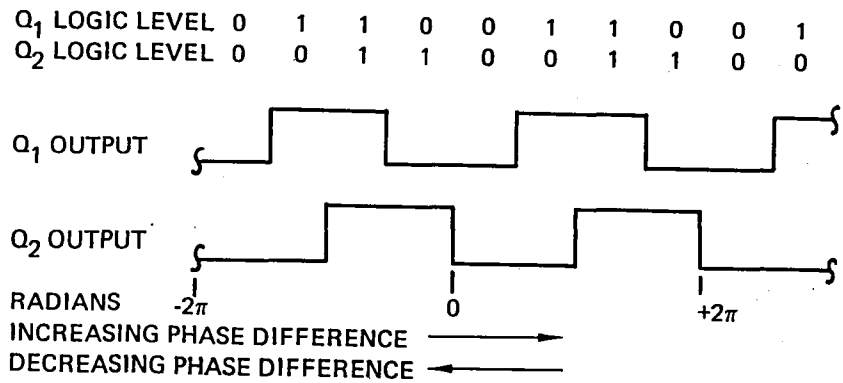

Figure 18: Quadrature Detection Transfer Function

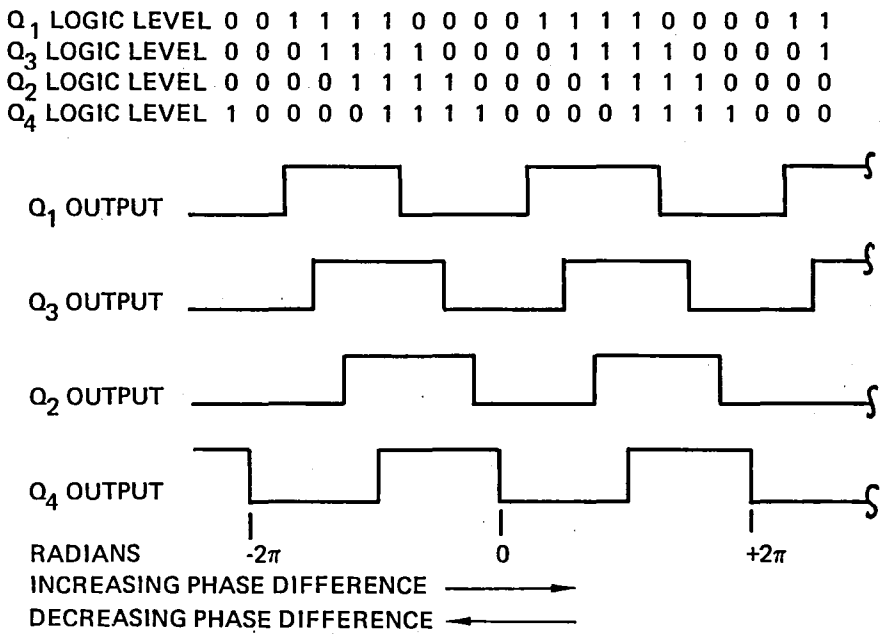

Figure 19: Multiple Quadrature Detection Transfer Function

tion determining the logic uses this unique repetitive sequence to determine the change in direction of phase. Use of quadrature detection results in fringe resolution of $\frac{\pi}{2}$ radians, one fourth of a fringe.

Multiple quadrature detection can be used to further divide the fringe. Figure 19 is a block diagram of multiple quadrature detection using a pair of quadrature detectors, where a fringe is resolved to $\frac{\pi}{4}$ radians, one eighth of a fringe. One quadrature detector is exactly the same as previously described. The other is also the same except the reference phases are shifted by $\frac{\pi}{4}$ radians relative to the other quadrature detector. Figure 20 is a representation of the transfer function for multiple quadrature detection using a pair of quadrature detectors. Note again that a unique repetitive sequence exists, resolving a fringe into eight elements. The direction determining logic uses this unique repetitive sequence to determine the change in direction of phase. For multiple quadrature detection a repeatable sequence occurs for every 2^n quadrature detectors used, where n is a positive integer, resulting in a fringe division of $2^{(n+1)}$. Fringe division is limited by this method by the analog to digital conversion process. The more quadrature detectors utilized to improve the resolution, the smaller the "window" that must be used for the analog to digital conversion. This has the undesirable equivalent effect of increasing the system bandwidth, requiring larger input signal-to-noise ratios.

Phase multiplication with quadrature detection uses quadrature detection as shown in Figure 21 and described above, except the input signal and reference phases are multiplied by some factor before application to the quadrature detectors. Phase lock loop, PLL, and successive squaring phase multiplication have been used on other angle measuring devices we have developed. With the

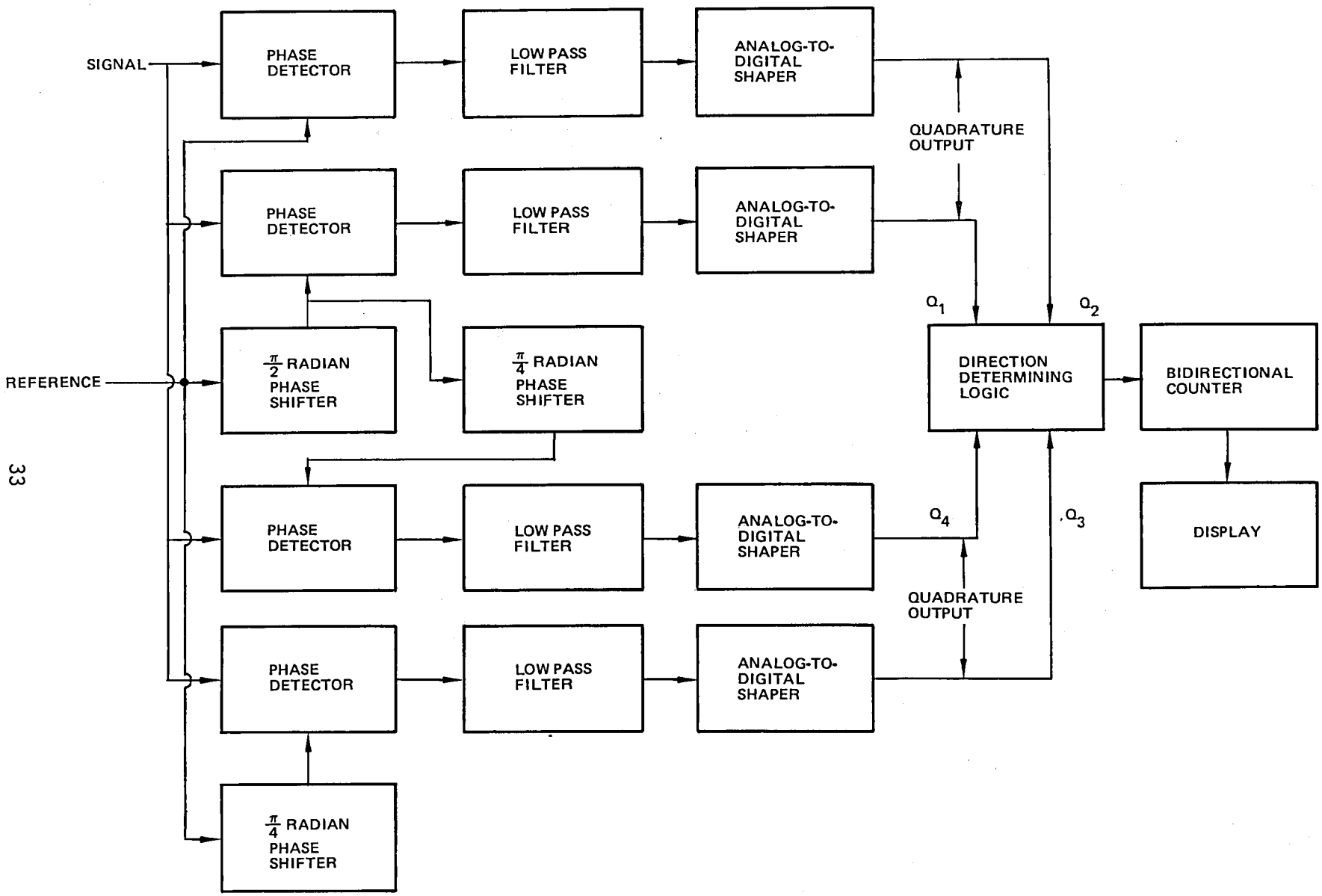

Figure 20: Multiple Quadrature Detection

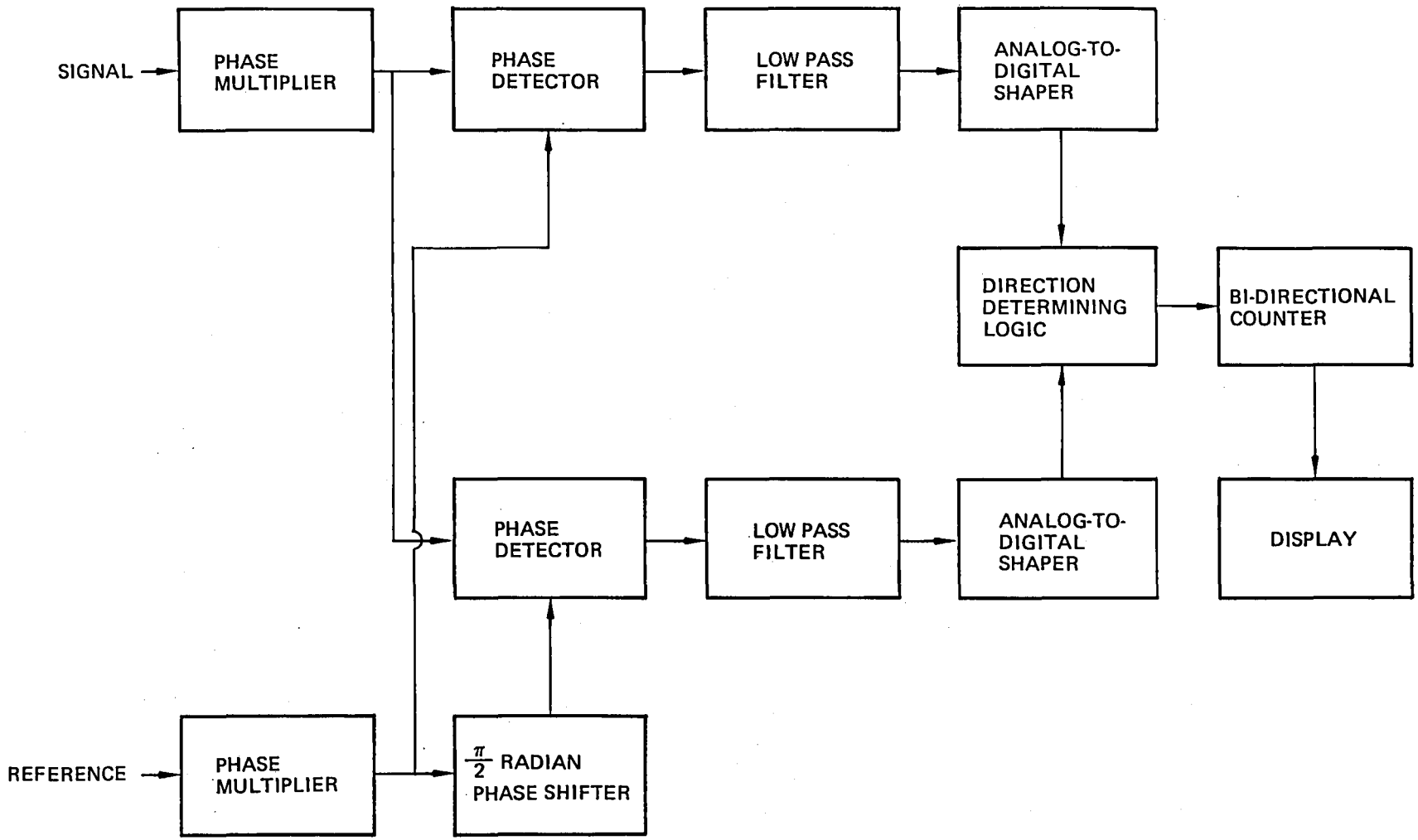

Figure 21: Quadrature Detection with Phase Multiplication

PLL multiplier, a PLL with the voltage controlled oscillator operating at a multiple of the input frequency and a divide chain to divide the voltage controlled oscillator down to the input frequency reused. Phase multiplication is done in the same way for the reference phase and phase modulated signal. With phase multiplication by successive squaring, frequency doubling is accomplished each time the successive outputs are squared. Phase multiplication of 2^n, where n is an integral number, occurs each time n successive outputs are squared.

The start and stop counter phase measurment method, Figure 22, uses a counter driven by a gated clock. The input to the counter is a clock frequency which is a multiple of the reference frequency and may or may not be phase locked to the reference frequency. The clock is gated into the counter at the time of zero crossing of the reference phase and continues to count at the clock rate until the clock is gated off at the next crossing of the signal phase. The total counts during this interval compared to the number of counts for one cycle of reference is a measure of the fractional part of a fringe cycle. A phase measurement can be made for every two cycles of reference frequency. Two counters are used. One counter is the instantaneous measurement of the fractional part of the fringe cycle and the other totalizes the whole fringe cycles.

The low operating frequency of the angle measurement system lends itself nicely to this method. For the two axis breadboard, circuitry was designed, fabricated, evaluated, and used for processing the signal from one axis. The other axis used the successive squaring method.

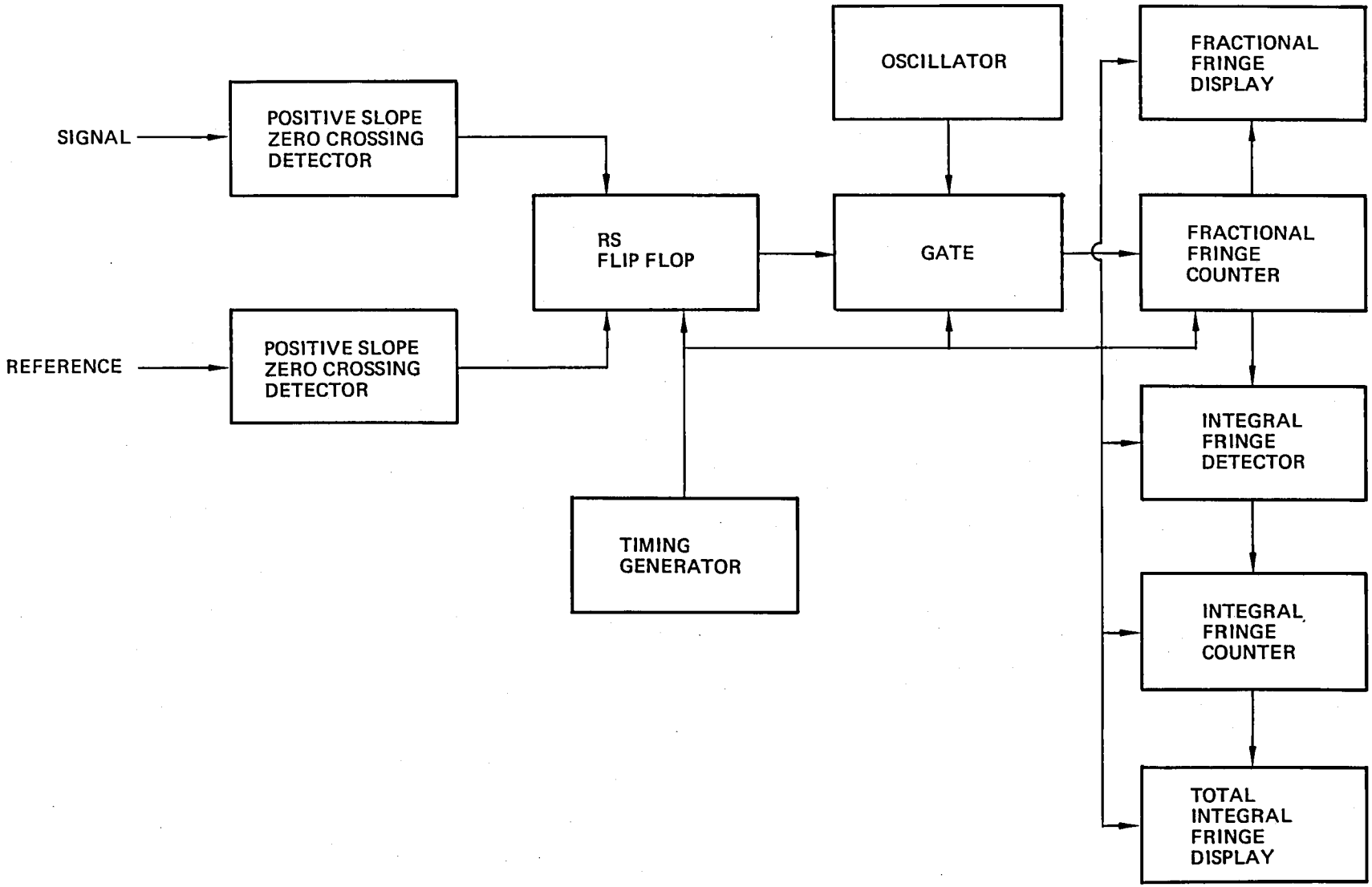

Figure 22: Start and Stop Counter Phase Measurement

When using the quadrature detection technique for phase measurement, any loss of signal accompanied by dynamic motion of the model results in erroneous angle measurement after the resumption of acceptable signal conditions. The fractional fringe angle measurement of the start stop counter method is affected during loss of signal only. The fringe summation counter can accumulate integral errors during loss of signal. In the breadboard evaluation of the start stop counter method, white noise was added to a simulated signal which was phase modulated at rates in excess of that anticipated by the NTF facility. No detectable errors were observed for signal-to-noise ratios in excess of two-to-one.

The two axis breadboard electronics used different processing methods for each axis. One axis utilized the successive squaring method of phase multiplication with quadrature detection and the other the start stop counter method of phase measurement.

Other pitch angle measuring devices we have developed have used PLL phase multiplication with multiplication factors of six. Lack of symmetry of the voltage controlled oscillator output required the loop to operate at twelve times the input frequency. A division of two provided the desired multiplication of six. Excessive phase jitter limits the use of PLL's to small multiplication factors.

Figure 23 is a block diagram of the successive squaring processor used in one axis of the breadboard electronics. Part of this circuitry was developed for another program which required a large bandwidth and a multiplication of sixteen. PLL multipliers were not used because of phase jitter, limited bandwidth, lock up time, and the error in phase needed for PLL operation. The

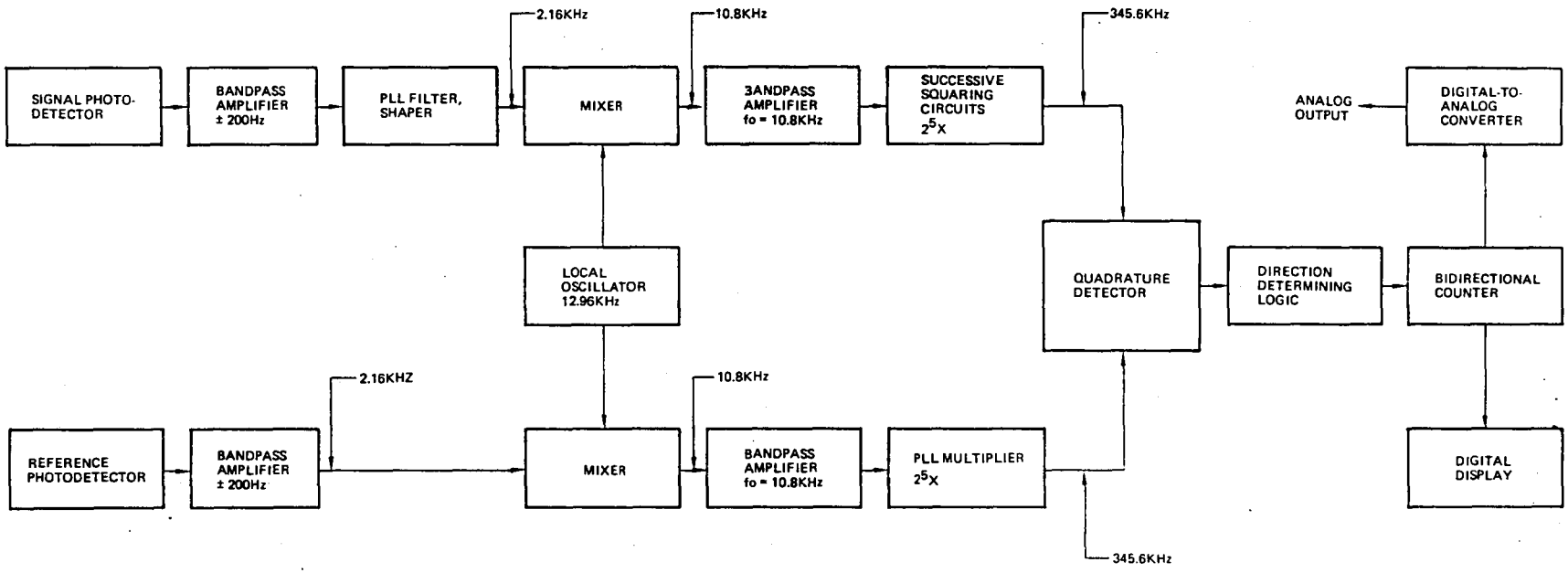

Figure 23: Block Diagram of the Successive Squaring Processor Used in the Breadboard.

input frequency of the existing circuitry was 21.6 KHz for a multiplication of 16. Since a resolution of around one-hundredth of a fringe was needed for the required angular resolution, another stage of squaring was added and the input frequency was changed to 10.8 KHz. This results in a resolution of 1/128 of the fringe angle.

Since the two axis breadboard operated at 2.16 KHz, two mixer circuits were used with a common local oscillator of 12.96 KHz for coherent frequency translation from 2.16 KHz to 10.8 KHz for the reference and signal. Figure 24 is a schematic of the successive multiplier circuit used for phase doubling. The output tuned circuit is used to filter out the undesired products of the squaring process. Measurement on the multiplier chain before addition of the needed doubler showed less than one count change for an input signal variation of 38 db and ± 3 counts for an input frequency variation of ± 500 Hz around a center frequency of 21.6 KHz.

Figure 25 is a block diagram of the start stop counter method of phase measurement used in the other axis of the breadboard. The output of the photodetector is amplified by a bandpass amplifier and applied to an automatic gain control, AGC, circuit. The dynamic range of the AGC circuit is in excess of 40 db. A limiter is used before the PLL to provide a fixed input amplitude to the amplitude sensitive PLL. The PLL is used as a combination bandpass filter and shaper since the output is digital. Phase measurements require a reference phase. The usual method of generating a phase reference has been with a light source, code disc, and detector. For the breadboard, an oscillator was used as the reference clock. From this reference, a 2160 Hz reference signal and the

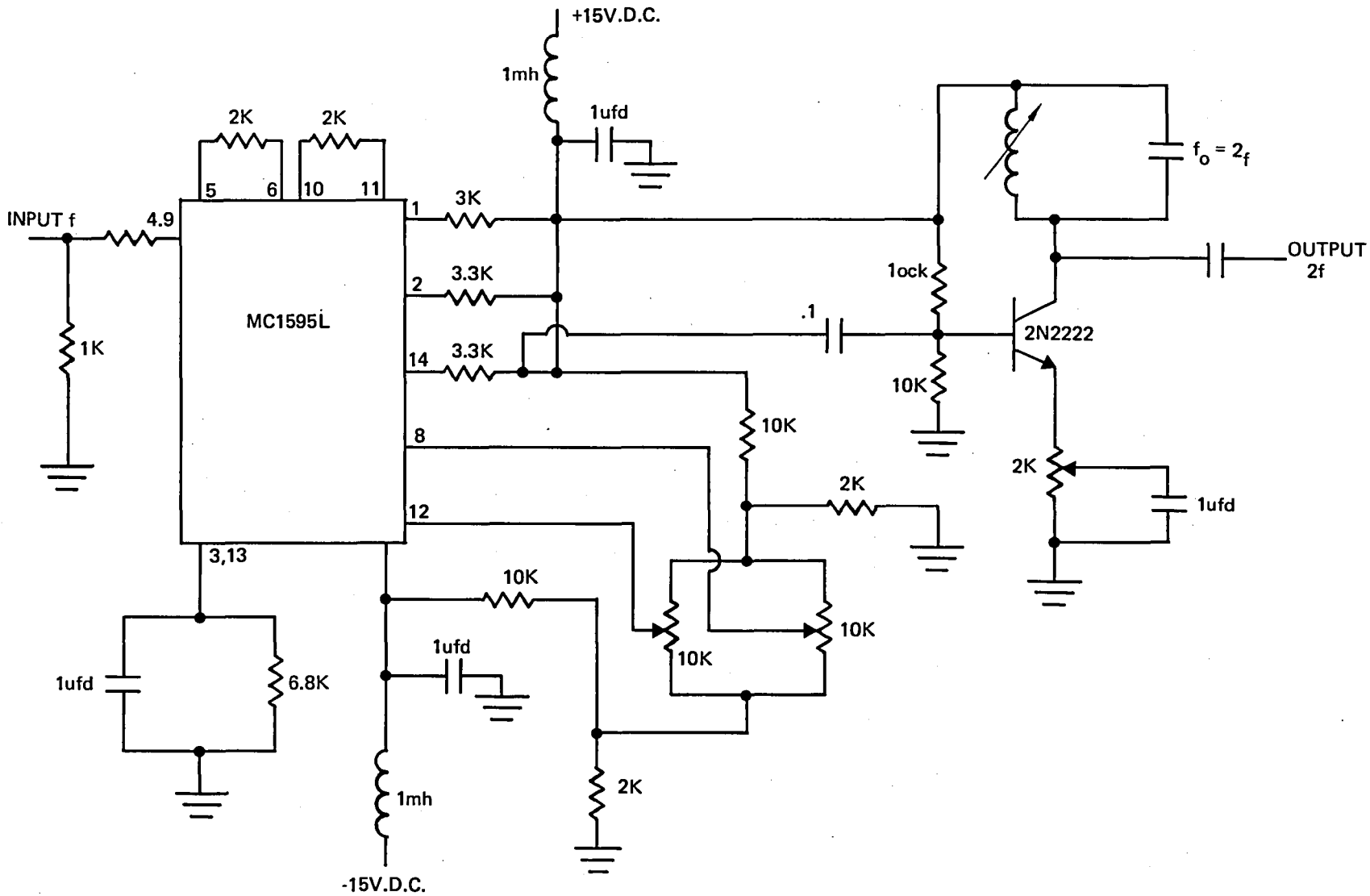

Figure 24: Phase Doubler

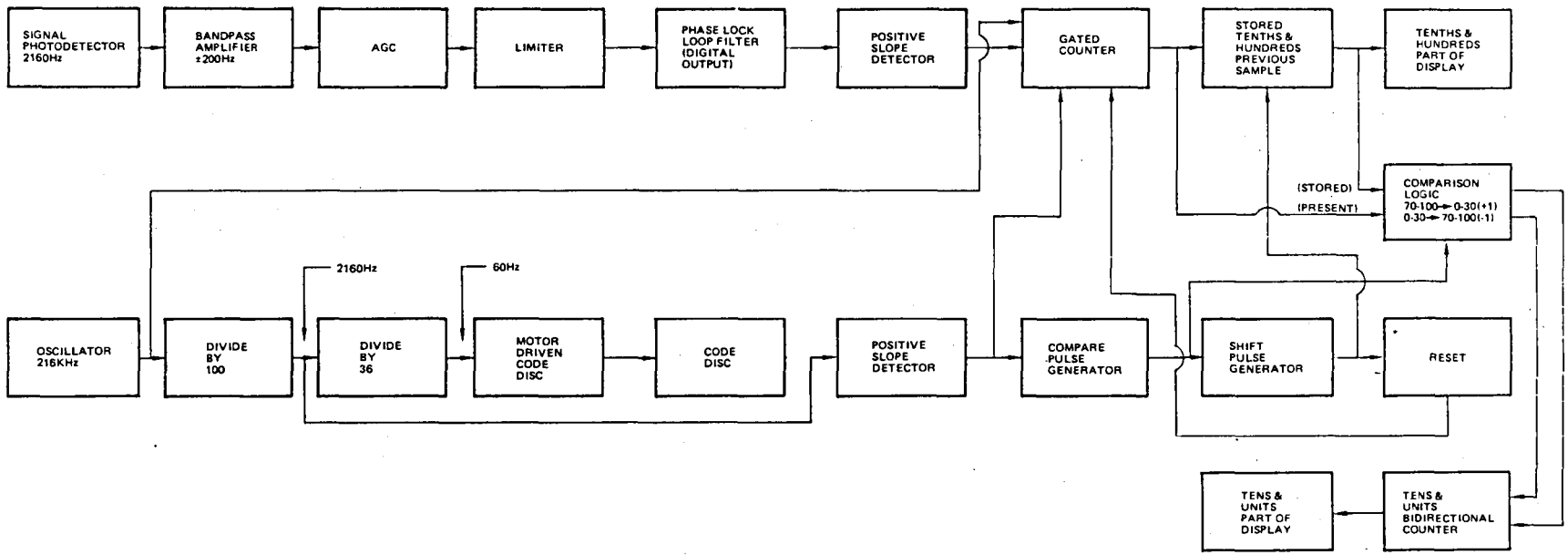

Figure 25: Block Diagram of the Breadboard Start Stop Counter Processor

60 Hz needed to drive the motor driven code disc were derived. The oscillator output was also used as input to the gated counter described below.

Phase between the input signal and reference is measured by measuring the time interval between zero crossing of the respective waveforms. The positive slope zero crossings were used for the breadboard. Figure 26 is a simplified timing diagram for the block diagram.

The sequence for making a measurement is as follows: The gated counter is reset to zero. The positive slope of the reference enables the gated counter, allowing it to count at the 216 KHz rate. The next positive slope of the signal stops the counter. Since there are 100 oscillator cycles for each cycle of the 2160 Hz reference, the counter indicates the phase difference between the reference and signal at the time of the measurement. The initial design fringe angle of the optical system was one degree, therefore, each count of the counter represent .01 degree. To allow processing time, a measurement is made every two cycles of reference, so the data rate (1080/second) is equal to one half the reference frequency.

The counter output represents the absolute phase difference between the signal and reference up to only one cycle of phase difference and then repeats for every cycle thereafter. Thus, the tenths and hundreds part of the display is the absolute phase angle between the signal and reference for each one cycle of phase difference. For increasing phase difference the counter output for successive data samples increases from 0 to 100 and repeats. For decreasing phase differences the counter output for successive data samples decreases from 100

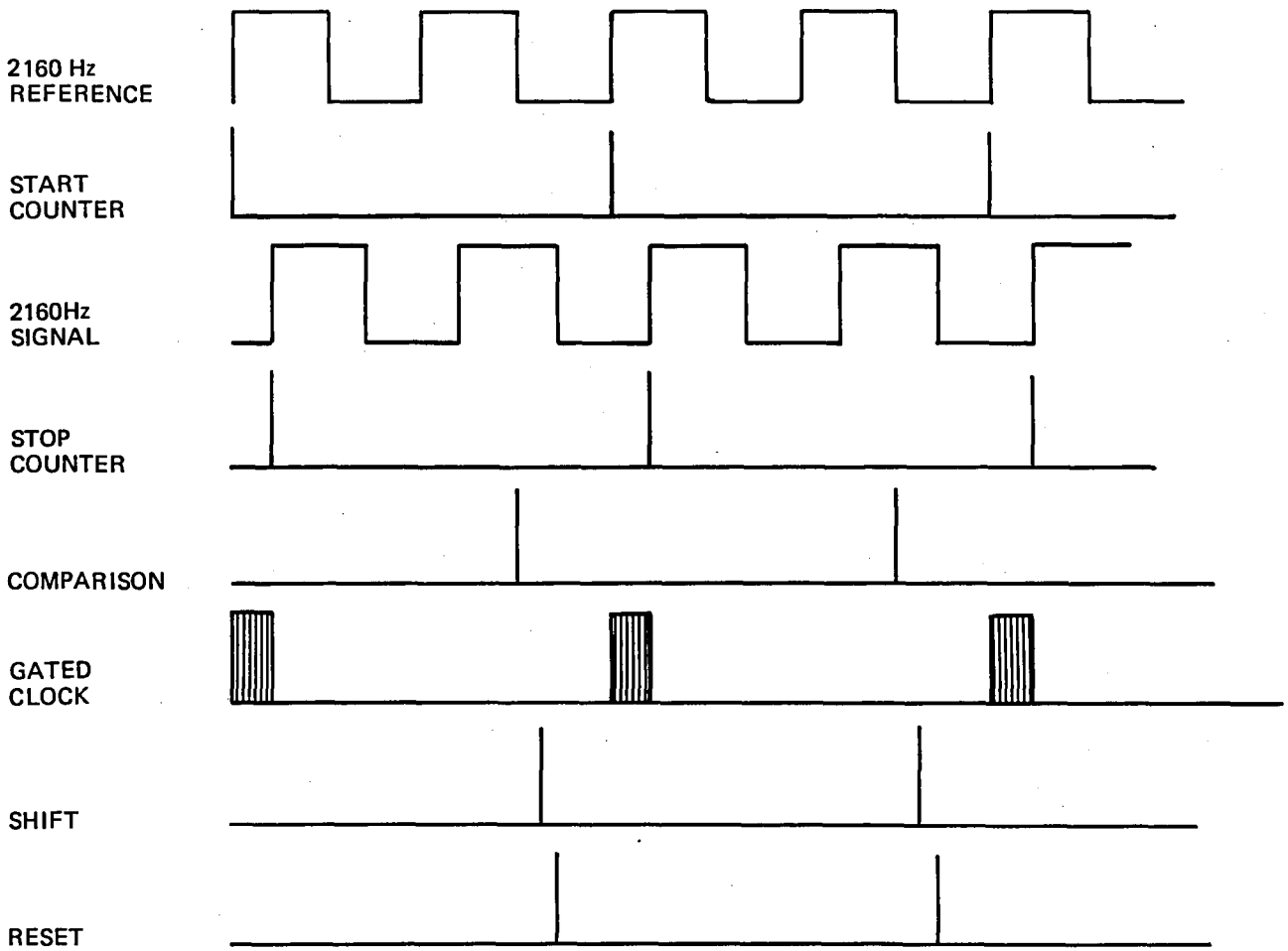

Figure 26: Simplified Timing Diagram for the Start Stop Processor

to 0 and repeats. This information is used to determine direction and to totalize the number of whole fringe cycles.

The present counter ouput is compared to the previous counter output by a comparison logic circuit. Since the counter output is the absolute fractional whole measurement only, the transition between whole fringes and the direction of transition must be determined. Whole fringe transition occur when the comparison between the present and previous data indicate a change from 100 to 0 for increasing phase differences and from 0 to 100 for decreasing phase differences. Because of fringe rates and noise, the comparison logic circuitry is designed to increment one fringe when there is a transition of the counter output (between successive samples) from 70 and 100 inclusive to 0 and 39 inclusive. If the transition of the counter output between successive samples is from 0 and 39 inclusive to 70 and 100 inclusive then this is a decrease of one whole fringe. The output from the comparison logic drives a bidirectional counter which totalizes the whole fringes. The output of the bidirectional counter is displayed as the tens and units part of the display. The outputs of the two counters can be combined to drive an analog output of pitch angle from a digital to analog converter.

Several conclusions were drawn from the evaluation of the breadboard electronics. For the start stop counter processor, all timing was initially derived from a 216 KHz oscillator including speed control of the code disc driven motor. It was found that the speed control varied significantly as a function of time, introducing instability and inaccuracy. Provisions had been included in the circuitry for use of an optical generated reference and this was used later. The reference and the oscillator were not synchronous but the frequency

of the oscillator was close enough to a factor of 100 of the optical generated reference so the error was no more than one count.

As mentioned before, any loss of signal accompanied by dynamic motion of the model results in erroneous angle measurement when using the PLL phase multiplication method or the successive squaring method. On the other hand, the fractional fringe angle measurement of the start stop counter processor is affected during loss of signal only. The integral fringe bidirectional counter will not produce an error unless the model moves one or more fringes during the loss of signal. Under adverse conditions, a coarse measurement may be required to redefine the integral part of the angle after loss of signal, but the fractional part is absolute.

The successive squaring and start stop counter processors were evaluated in parallel using a common reference and signal. Bandwidth limiting of the signal up to the squaring circuits and input to the stop start processor were identical. Random noise from a General Radio Type 1390-B noise generator was linearly added to the signal before bandwidth limiting. A Hewlett Packard variable phase function generator model 203A and a Wavetek model 180 sweep function generator were used as signal sources. The phase of the signal was varied for different input signal-to-noise ratios and the errors were recorded over time intervals from 5 to 30 minutes. Operation of the start stop processor was greatly superior to the successive squaring processor. For signal-to-noise ratios greater than two, no errors were detected for the time intervals mentioned above for different phase conditions. Figure 27 shows oscilloscope traces for a signal-to-noise ratio of two. Figure 27-a is the wideband summation of the signal and noise. Figure 27-b is the bandlimited signal into the

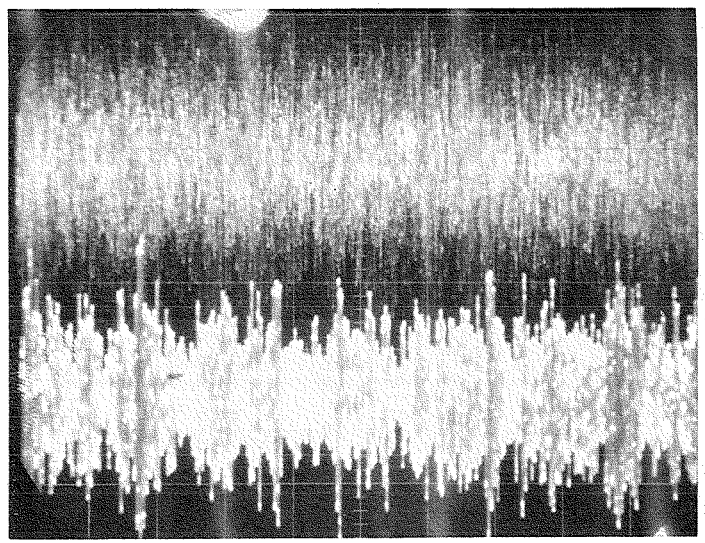

(a) V = .5V/div
H = 10msec/div
WIDEBAND SIGNAL + NOISE

(b) V = .5V/div
H = 10msec/div
NARROWBAND SIGNAL + NOISE

(c)

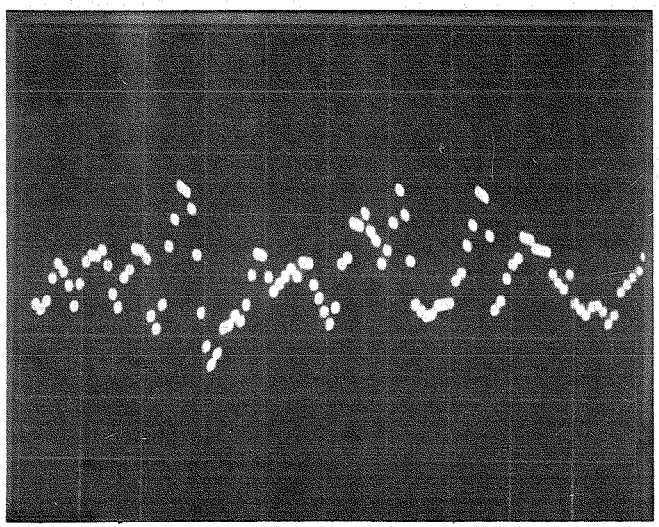

V = 10mv/div
H = 10msec/div

ANALOG OUTPUT 0°/sec RATE

(d)

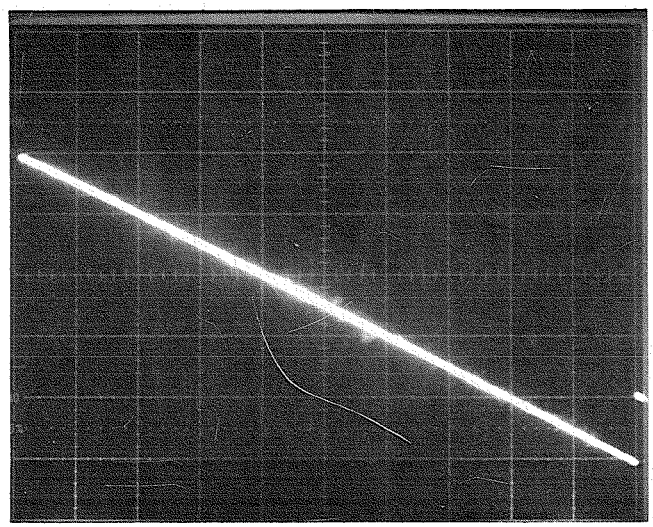

V = .5V/div
H = 40msec/div

ANALOG OUTPUT FOR SIMULATED 200°/sec RATE

Figure 27: Photographs of S/N Measurements

processor. The signal-to-noise ratio was measured at this point. Figure 27-c is the analog output for the same time interval as Figures a and b. Figure 27-d is a picture of the analog output for a simulated angular rate of approximately 200 degrees per second for a signal-to-noise ratio of two.

High resolution fringe counting interferometers of the type used in the laser angle sensor usually exhibit a slight sinusoidal small-scale nonlinearity. This can be due to (1) electrical coupling between the signal and reference channels (through a common power supply, for instance), (2) optical coupling due to spurious reflections, or (3) improper illumination of the scanning element at the focal plane of the collimating lens.

The output of the breadboard system was checked at 4 arc-minute steps over a 2^{o} increment using a Wild T-2 theodolite. The signal from the vertical detector was fed into a multiple squaring type processor (#1) and a counting type processor (#2). The fringe angle was 0.354 degrees.

Figure 28 shows the indicated angle output as a function of the theodolite angle. The small scale nonlinearity is not evident on the scale shown in the figure. Figure 29 has a greatly expanded scale showing the angular output of the processors about a best-fit line. All the data is within $\pm$0.01 degrees of the best-fit line. As expected, the data varies in a sinusoidal manner with a period of 0.35 degrees. Note that signal characteristics (amplitude and phase) are essentially independent of the signal processor. This indicates that in this case, the small scale nonlinearity is caused by optical coupling rather than electrical coupling.

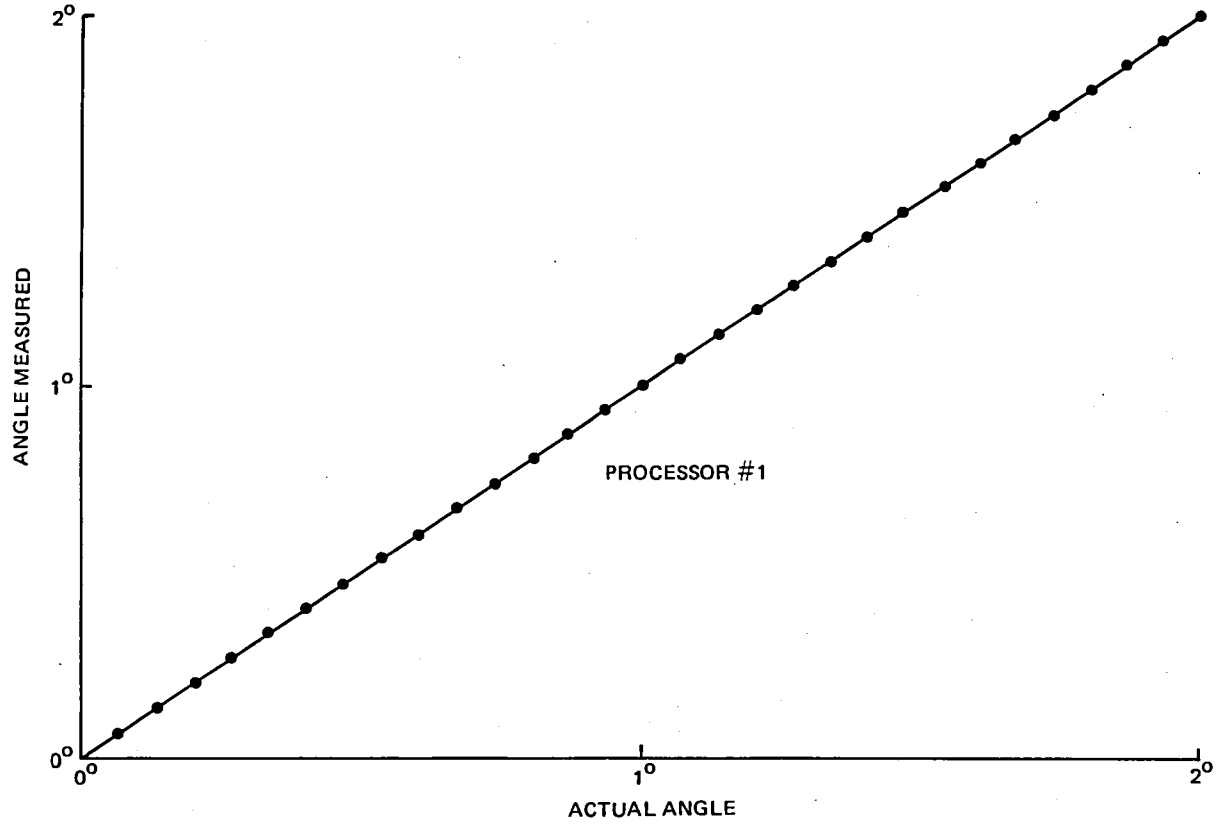

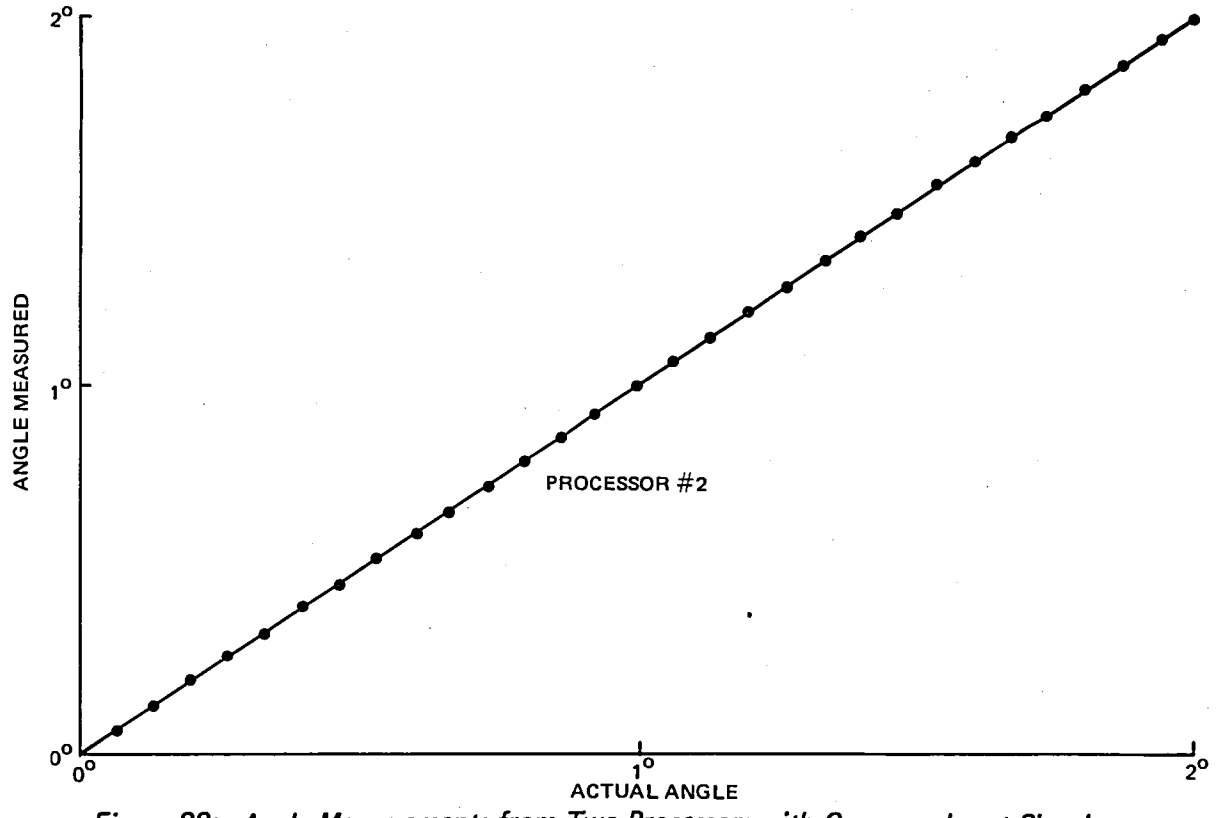

Figure 28: Angle Measurements from Two Processors with Common Input Signals

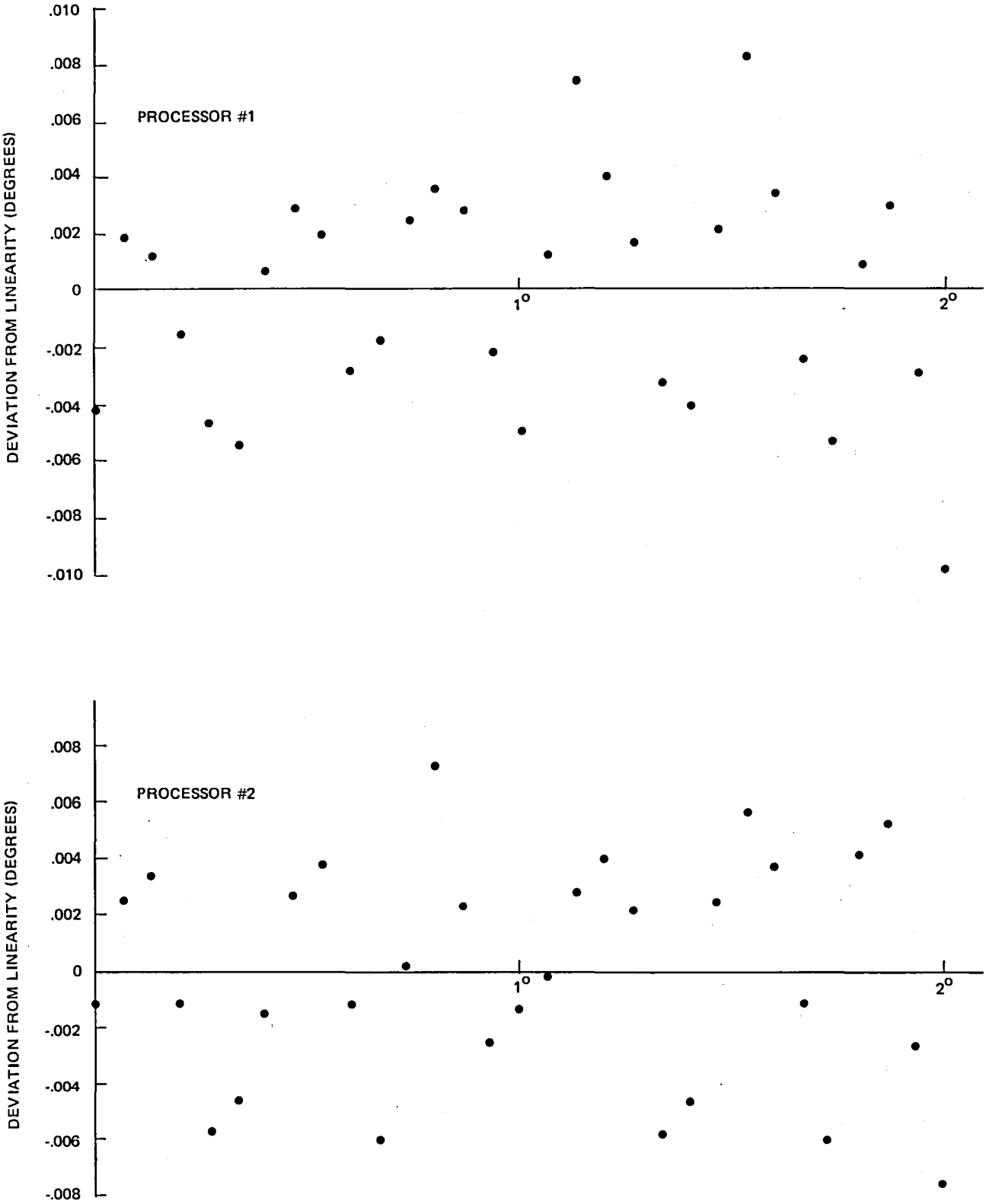

Figure 29: Deviation from Best-Fit-Line

V. PRELIMINARY DESIGN

The results of the breadboard experiment, distortion measurements, and window technology studies were used to develop a preliminary design (PD) for a two-axis laser angle sensor. The two-axis PD includes expected specifications, descriptions of the optics and electronics, NTF installation geometry, insulation and thermal control, and NTF interface requirements.

Figure 30 shows the general layout of the optical head mounted inside a structural beam above the test section of the NTF. The optics are enclosed in a pressure tight package covered with 2.5 cm of exterior insulation. The unit is inserted through an access slot on the upper part of the beam and bolted to the side rails.

As in the breadboard system, the helium-neon laser beam (λ = 633 nm) illuminates the lens disc in two places to form scanning sources for pitch and roll measurement. As discussed in Section IV, the scan direction is 45^{o} from the flow direction. The dove prism rotates the pitch source 90^{o} relative to the roll source. The beams are orthogonally polarized and then combined with a beamsplitter. Part of the outgoing beam is sampled with the reference detector. The reflector assembly consists of pitch and roll reflectors. Sheet polarizers on the face of each reflector are oriented to pass the polarized pitch and roll beams. The return beams are separated by a polarizing splitter into pitch and roll beams. A mask on the face of each detector selects the proper diffracted order (-1, 0, or -1). Extraneous light is reduced with a narrow band spectral filter. The signal and reference voltages are amplified with buffer amplifiers and relayed to the control room for processing.

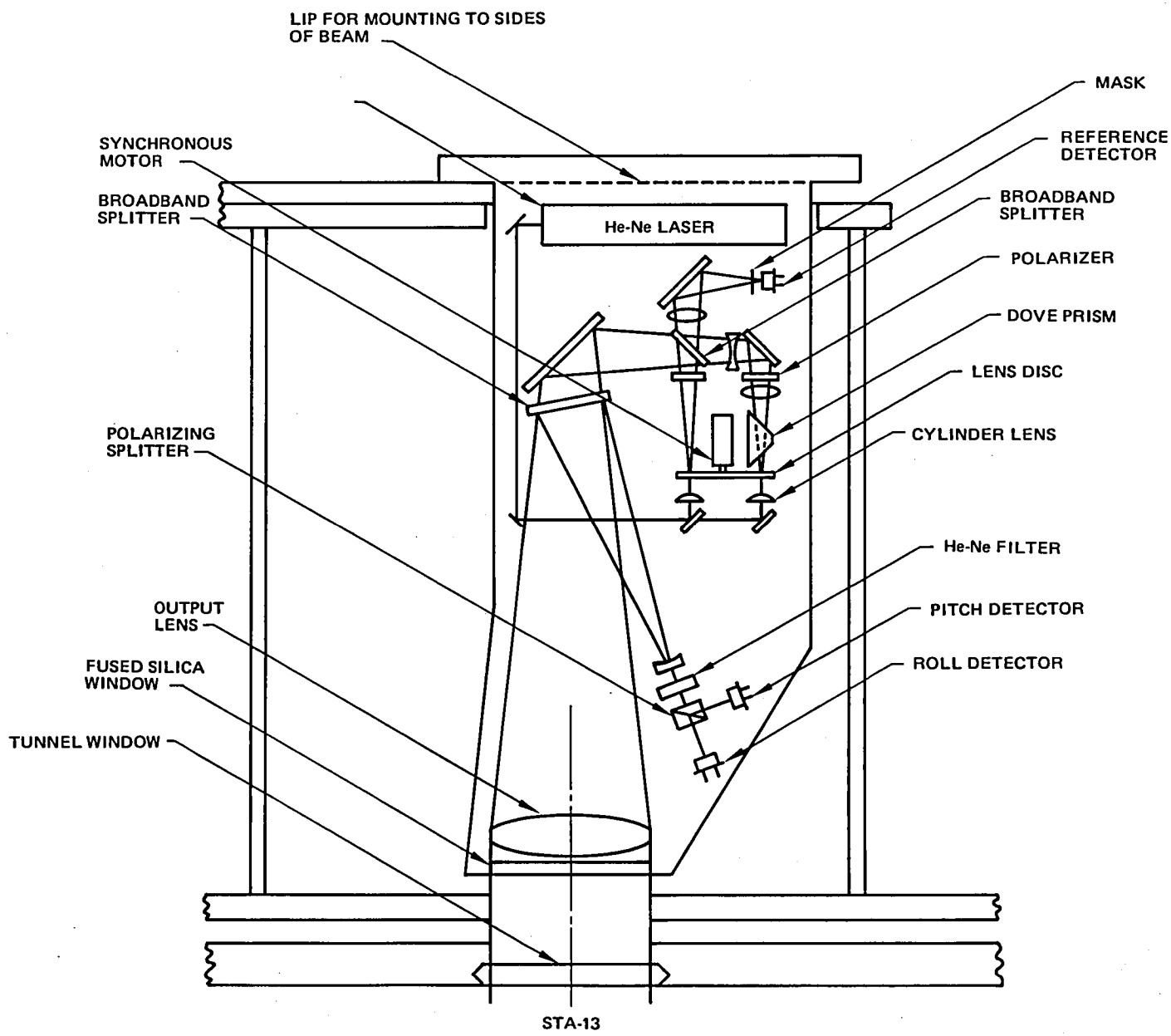

Figure 30: Optical Schematic of NTF Installation

Figure 31 is a cross-section of the reflector assembly looking down the model axis. The figure shows the window mounted to the skin of the model and the reflector mounted to a strongback inside the model. Other arrangements are possible, such as mounting both window and reflector to the skin, but the arrangement shown illustrates one solution to the thermal problems of the reflector and the windows.

The window is glass, approximately 3 mm thick with a 12.5 mm clear aperture. The window is curved on both surfaces, where the outer shape matches the shape of the model. The thermal expansion coefficient of the window is approximately equal to the expansion coefficient of the skin. Differential expansion and point stress on the window are relieved with compliant gaskets of high expansion material (such as teflon) at the window edges. The beveled edges of the window are conical shapes that can be ground on a lathe. The mating retainer ring surfaces are also conical, so both the outer edge and inner surfaces of the window retainers can be made on a lathe. The window retainers can be held by screws (not shown).

The retroreflector housing is a flanged cylinder with an opening at the top. The hologram and cube corner retroreflector are held in place by conical springs below the reflector seat. Hologram rotation is prevented by forcing a small amount of epoxy down between the glass edge and the housing. A pair of dowel pins assures proper orientation of the housing relative to the model axis.

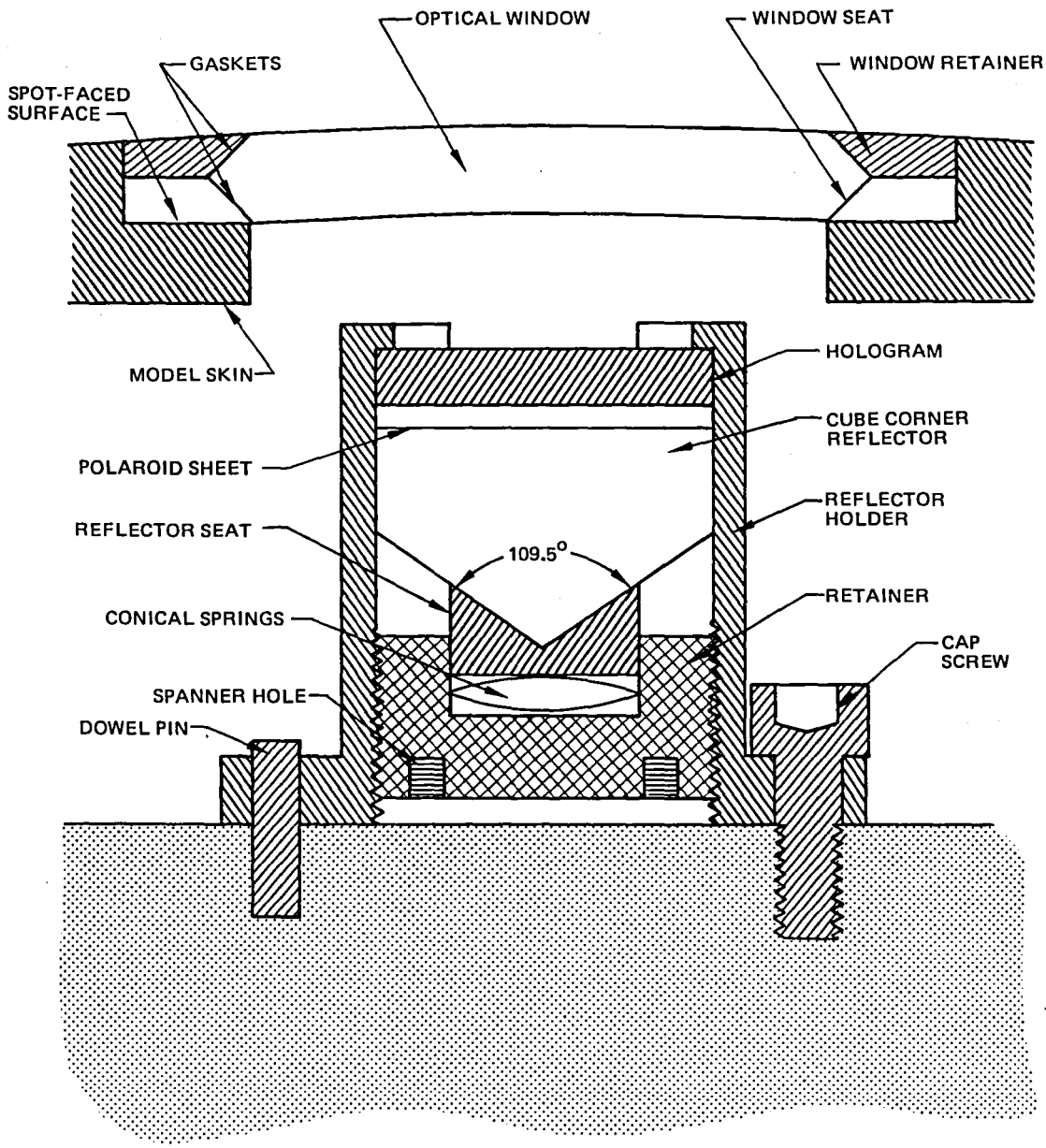

Figure 31: Reflector Assembly and Window

The temperature of the reflector assembly and density of the tunnel GN_2 will vary during operation of the tunnel. If the hologram substrate and retroreflector are made of the same glass, the effects of thermal expansion are essentially eliminated, since the change in hologram spacing compensates for the change in retroreflector height. However, the index of refraction of glass changes with temperature and the index of refraction of the GN_2 changes with density. Both effects produce a zero-order fringe shift F(i) given by

$$F(i) = \frac{2h}{s} \tan \left[\sin^{-1} \left(\frac{n_g}{n_r} \sin i \right) \right]$$

where

h = reflector height

i = angle of incidence

n_g = index of refraction of the GN_2

n_r = index of refraction of the glass (1.52 for BK7 glass)

s = hologram fringe spacing

In order to estimate the correction factor, suppose that the tunnel is operated at high pressure and cryogenic temperature where the density increases by a factor of 24. Refractivity (n_g-1) is proportional to density, so the index of refraction increases from 1.0003 to 1.007. The index of refraction of the reflector also changes, but the effect is only about 1 part per million (for BK7 glass) at room temperature, decreasing rapidly as the temperature is reduced. The dominant effect is the change in refractive index of the nitrogen gas. Let F' denote the fringe count at high pressure and low temperature, then

$$\frac{F'}{F} = \frac{\tan\left[\sin^{-1}\left(\frac{1.007}{1.52}\sin 20^{0}\right)\right]}{\tan\left[\sin^{-1}\left(\frac{1.003}{1.52}\sin 20^{0}\right)\right]} = 1.00706$$

The uncorrected angle indication is 20.14^{0} instead of 20^{0}. Since the correction is small, only a rough measurement of GN_2 density is required. Note that the effect changes the slope of the calibration curve. There is no zero shift due to varying GN_2 density.

Electronic Processor:

Figure 32 is a general block diagram for the proposed processor electronics. An HP-85 desktop computer with an HP-IB interface card will be used in the system to perform linearization, table storage, automatic calibration, control functions, calculations, and output the pitch and roll angles as a function of time. Uncorrected angle measurement independent of the HP-85 will be available and can be displayed. Use of the HP-85 and the HP-IB interface will allow usage of the basic angle measuring device with other computing devices that utilize the IEEE-488 standard interface. The following is a general description of the block diagram for the proposed processor electronics.

The electronics for the two axes are identical, except for the electronics in the reference channel preceeding the PLL. The reset function is common to both sets of electronics. Signals Sp, S_r, and R will be conditioned by bandpass amplifier line drivers where S_p, S_r, and R are pitch signal, roll signal, and reference signal respectively. Three line drivers will drive twisted pairs of

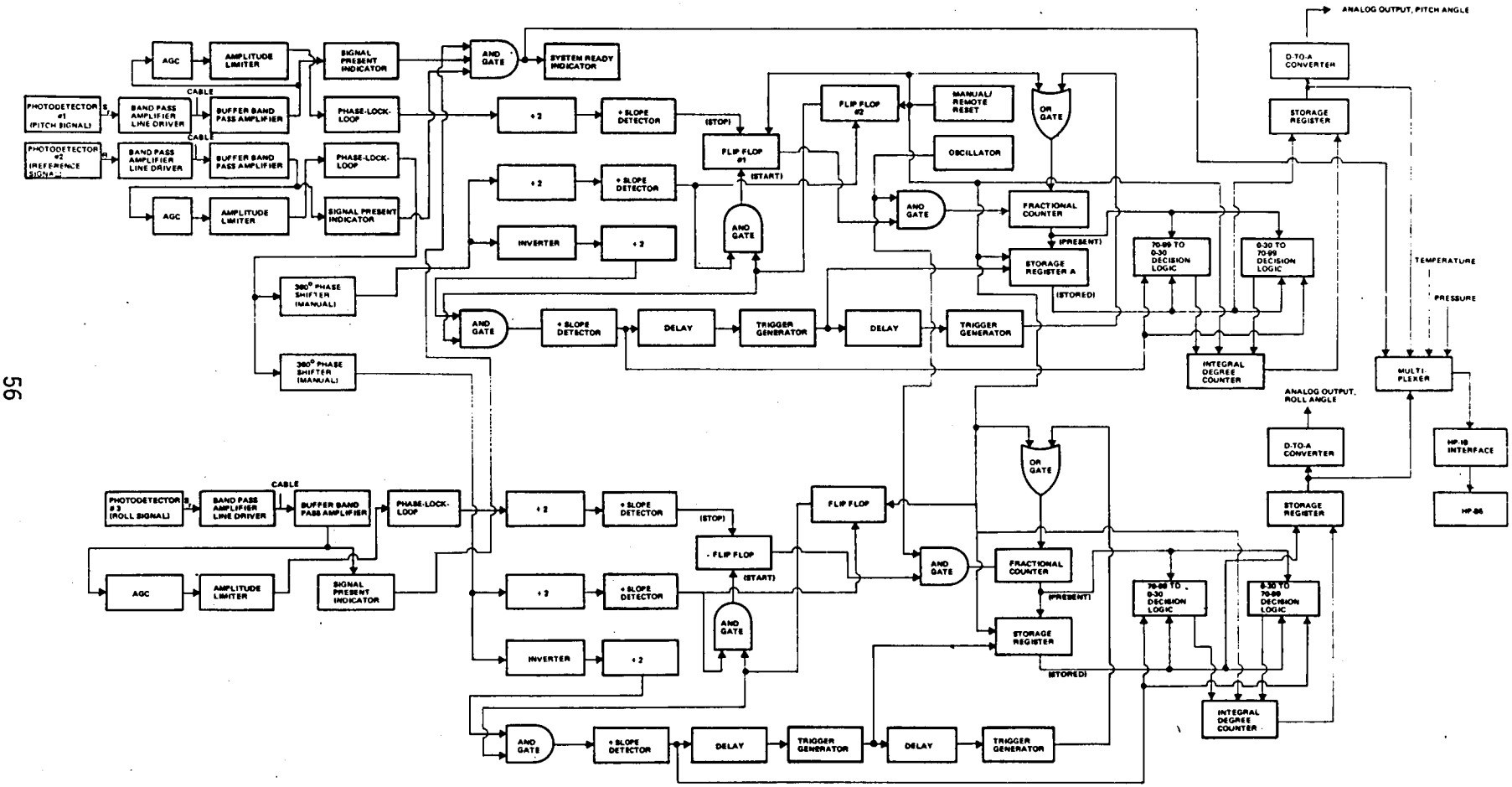

Figure 32: Block Diagram of Proposed Two-Axis Processor

a multi-conductor cable leading to the processor electronics. The processor can be located up to 200 feet from the optical assembly.

The inputs to all buffer bandpass amplifiers will be transformer coupled to minimize ground loops and cable pickup. Signal presence of a predetermined threshold is determined for S_p, S_r, and R. System ready indication (when the three signals are present) is also sent to the computer. All channels will have a minimum of 40db of automatic gain control to allow for conditions of fog and laser output degradation. The reference channel will have a manual phase adjustment for each axis. The phase can be varied over 360 degrees. To minimize input amplitude effects on the output of the phase lock loops filters, amplitude limiting is provided before the PLL. The output of the PLL's to be used will be digitally compatible with standard transitor-transistor logic. The analog to digital conversion is done by the PLL. Up to the outputs of the PLL's, channels S_p, and S_r are identical. Up to this point only input signal conditioning has taken place, basically filtering and digital conversion for the three channels. The actual phase measuring circuitry follows the PLL's.

The phase measurement method using a start stop counter will be used to derive the phase information. This method was evaluated as part of the breadboard circuitry. The phase measurement is made by continually measuring the time that elapses between the zero crossing for a specific slope of a reference signal and the zero crossings for a specific slope of the signal whose phase is to be measured relative to the reference.

The processing of one axis will be described since both axes are identical. A phase measurement is made every two cycles of the reference frequency resulting in a data rate of one half the reference frequency. The PLL output of the reference channel drives a phase shifting circuit by which the reference phase can be manually adjusted over 360 degrees of phase difference. Each axis has its own phase shifter. This adjustment will be used for initial zero angle adjustments.

Timing for the logic operations is derived from the reference signal. The phase shifted output from the respective axis is divided by two and a slope detected (a positive slope is indicated). The pulse generated by the slope detector will be the start pulse which occurs every two cycles of reference. The same output from the phase shifter is inverted, divided by two, and a slope is detected. This provides a reference signal which is in quadrature with the divided and noninverted reference. The slope of the quadrature reference which is one and a half cycles later than the non-inverted reference is detected and used for timing. The slope detector output of the delay element initiates a trigger generator which strobes the storage register, transferring the contents of the fractional counter into the storage rejector. The trigger initiates another delay element initiating another trigger generator. The output of the trigger generator resets the fractional counter to zero. The time delay for the delay elements are very small compared to a quarter cycle of reference. Figure 26 is a timing diagram applicable to the description above and below. Further description of the processor and its relationship to the timing follows.

The system is reset by the manual or remote reset. This inhibits flip flop number one as if it had received a stop pulse from the signal slope detector. Note that the signal is also divided by two before the slope is detected. The manual or remote also sets the fractional counter gate, the storage register A, and the integral degree counter to zero. It also sets flip flop number two which inhibits the and gate input to flip flop number one. This inhibits the reference start pulse previously described from operating on flip flops one and two.

Removal of the reset command enables flip flop number one, the fraction counter, storage register A, and the integral degree counter. This also enables flip flop number two so the next positive slope of the reference will trigger it allowing a synchronous reset with the reference phase. The output of flip flop number two enables the and gate allowing the same positive slope of the reference to trigger flip flop number two. The output of flip flop number two changes state enabling the and gate input to the fractional counter causing the counter to count at the oscillator frequency. The positive slope of the signal channel, which occurs after the positive slope of the reference channel, causes the output state of flip flop number one to change and inhibits the and gate input to the fractional counter causing the counter to stop counting. As described above the output of the positive slope detector in the timing chain occurs one and a half cycles of reference after the reference positive slope is detected. By this time a stop pulse must have occurred even for the lowest anticipated doppler frequency. This timing pulse strobes the decision logic circuit.

In the decision logic circuitry a comparison is made between the output of the fractional counter and the output of the storage register. The output of the fractional counter is labeled present and the storage register stored. During the reset described above the storage register was reset to zero so the first comparison of the fractional counter output after reset is made with the register output equal to zero. The numbers shown in the decision logic blocks of Figure 26 are for an oscillator frequency equal to one hundred times the reference phase and synchronous with it. If the number in the stored register is anywhere between 0 and 39 (in this case 0 because of the reset) and the present is anywhere between 70 and 99, a pulse will be inputed to the integral degree counter. The integral counter will now have one count less, equivalent to one degree less. The measured angle is thus the integral counter output plus the fractional counter output. If the present number was anywhere between 0 and 39 then the integral counter would not be increment by one. Excluding the first measurement after reset, if the number in the stored register is anywhere between 70 and 99 and the present is anywhere between 0 and 39 a count will be added to the integral counter. Again the measured angle is the sum of the integral counter and the fractional counter. The next trigger in the timing chain shifts the output of the fractional counter into the storage rejector. The last trigger resets the fractional counter through the on gate. The next reference positive slope start pulse, cases flip flop number one to change state and measurement cycle repeats. Storage registers are used to store the fractional and integral counter outputs.

The outputs of the pitch and roll axes are combined in a multiplexer and approximately timed for interfacing with the HP-85. Temperature and pressure inputs will also be provided to the multiplexer interface. These will be used for computation of the corrected angle.

Environmental Control:

This section is a discussion of the environmental conditions required within the optical head. The basic decision is whether to keep the optics at near ambient temperature and pressure, or to allow the temperature and/or pressure to follow the plenum environment.

Concerning temperature, the optical unit must be held at near constant temperature simply because of the cost to design, fabricate, and test an optical instrument of this complexity that could function reliably when the temperature changes repeatedly from above room temperature to cryogenic temperature. The insulation and heat transfer requirements are discussed later in this section.

The trades between venting the optics to the plenum or maintaining constant pressure are listed below.

Constant Pressure:

(1) The housing must withstand the pressure load.

(2) A pressure window is required. This can be the output lens or a separate window.

(3) The increased wall thickness required for the housing reduces space available for the optics.

Vented to Plenum:

(1) The incoming nitrogen gas must be heated or cooled to the temperature of the optics.

(2) Optical effects due to density (defocusing, laser misalignment, change in refraction angles, etc.) must be analyzed and appropriate adjustments made to the calibration equation.

(3) There are several mechanical effects to consider, such as venting the space between elements of the air-spaced output lens and increased aerodynamic drag on the rotating lens disc due to density.

(4) The electronics in the optical head must survive repeated pressure fluctuations.

It appears that long-term reliability goals can best be served by keeping the optics at constant pressure (and temperature).

The heat transfer requirements to keep the optics at 300°K when the plenum temperature is 100°K are now estimated. Assume an ideal porous insulator on the outside of the housing, where the thermal conductivity is equal to the conductivity of GN_2. Over the range of NTF conditions, the thermal conductivity of GN_2 is approximately

$$k \cong (1.1 \times 10^{-5} + 8.3 \times 10^{-7}\ T)\ w/cm\text{-}^{o}K$$

where T = temperature in °K

Let Q = heat flow in watts/cm^2

T_o = plenum temperature

T_i = interior temperature

h = insulation thickness

then $Q = \frac{kdT}{d^x}$ = heat loss per unit area

$$\text{and } \int_0^h Q \, dx = \int_{T_o}^{T_i} k \, dT$$

The heat flow is constant under steady-state conditions, so

$$Qh = \int_{T_o}^{T_i} (1.1 \times 10^{-5} + 8.3 \times 10^{-7} \, T) \, dT$$

$$= (1.1 \times 10^{-5} \, T + \frac{8.3 \times 10^{-7}}{2} T^2) \Big|_{T_o}^{T_i}$$

Take $h = 2.54$ cm

$T_o = 100^oK$

$T_i = 300^oK$

Then $Q = .014$ w/cm^2

The outside area of the optical head will be of the order of one square meter and a real insulator may be only 50% efficient, giving a total heat loss of 280 watts. The heat dissipation of the electronics in the head will be about 50 watts, so the heating requirement is of the order of 230 watts.

NTF Interface:

Figure 33 is a diagram of the anticipated interface between the angle measuring system and the NTF. All cables and connectors between the optical assembly and the tunnel wall will be provided by NASA and installed by Boeing. Connectors on the outside wall will be provided by NASA and the cables to the laser angle measuring electronics drawer will be made up by Boeing. NASA will provide the analog and digital output connectors from the drawer and provide or specify the interfacing cable. The heater controller for the heater in the optical assembly will be provided by NASA. If such a heater controller is not available at Boeing during development of the system NASA will provide Boeing a controller.

1. HP-85 Computer with HI-IB interface and I/O ROM memory
2. Cable connectors
3. Heater controller
4. Drawer panel
5. Analog output connector
6. Digital output connector

These items are to be available within two months after the starting date of the program.

Specifications:

The projected specifications of the two-axis laser angle sensor are listed in Table 3 below. These may be modified slightly to accommodate design constraints.

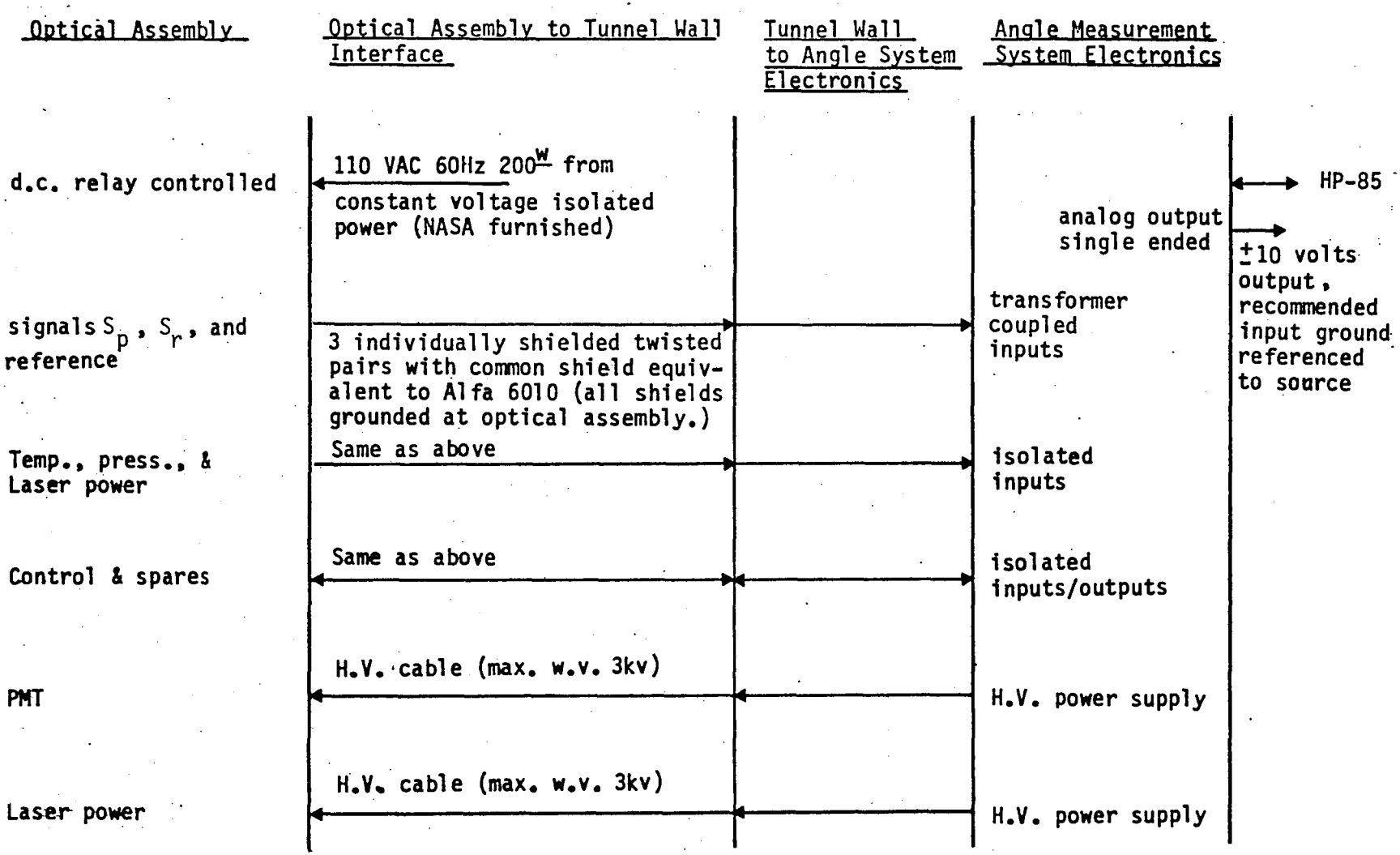

Figure 33. Anticipated Angle Measurement System Interfaces with NTF

Table 3 - Laser Angle Sensor Specifications

Angle Measurement	
Fringe angle	0.5 degrees
Angular resolution	0.005 degrees
Maximum angle rate	150 degrees/sec
Angular range	$\pm$20 degrees
Physical Characteristics	
Exit aperture of optics	6 x 13 cm
Working distance	0 to 5 meters
Effective beam size at 1.25 meters	6 x 9 cm

As listed in the table, the fringe angle will be 0.5^{o}. However, the system will be designed so that a change to 1^{o} can be made if required, depending on the actual wavefront distortion in the NTF. If the fringe angle is changed to 1^{o}, the resolution will increase to 0.01^{o} and the effective beam size at the model will be 6 cm square.

1. Report No.	2. Government Accession No.	3. Recipient's Catalog No.
NASA CR-159385		

4. Title and Subtitle	5. Report Date
LASER ANGLE SENSOR DEVELOPMENT	6. Performing Organization Code
7. Author(s)	8. Performing Organization Report No.
C. R. Pond and P. D. Texeira	10. Work Unit No.
9. Performing Organization Name and Address Boeing Aerospace Company P. O. Box 3999 Seattle, WA 98124	11. Contract or Grant No. NAS 1-15987
12. Sponsoring Agency Name and Address National Aeronautics and Space Administration Washington DC 20546	13. Type of Report and Period Covered Contractor Report, 1979/80
	14. Sponsoring Agency Code

15. Supplementary Notes

Contract Monitor: Tom Finley, NASA Langley Research Center

16. Abstract Electrical and optical parameters are developed for a two-axis (pitch/roll) laser angle sensor for the National Transonic Facility (NTF). The laser angle sensor is a fringe counting interferometer, where interference fringes are generated by a small passive reflecting element on the model. The laser source and detector are mounted in the plenum above the model. Two-axis optical distortion measurements of flow characteristics in the NASA 0.3-miransonic cryogenic tunnel were made with a shearing interferometer. The measurement results provide a basis for estimating the optical parameters of the laser angle sensor.

Experimental and analytical information was generated on model windows to cover the reflector. A two-axis breadboard was assembled to evaluate different measurement concepts. The measurement results were used to develop a preliminary design of a laser angle sensor for the NTF. Schematics and expected performance specifications are included in the report.

17. Key Words (Suggested by Author(s))	18. Distribution Statement
Angle measurement, wind tunnel instrumentation, interferometry	Unclassified-Unlimited

19. Security Classif. (of this report)	20. Security Classif. (of this page)	21. No. of Pages	22. Price*
UNCLASSIFIED	UNCLASSIFIED		

For sale by the National Technical Information Service, Springfield, Virginia 22161

End of Document